JOURNAL OF COLLOID AND INTERFACE SCIENCE 167, 47–65 (1994)

Capillary Image Forces

I. Theory

PETER A. KRALCHEVSKY,*[,1] VESSELIN N. PAUNOV,* NIKOLAI D. DENKOV,* AND KUNIAKI NAGAYAMA†

* *Laboratory of Thermodynamics and Physicochemical Hydrodynamics, Faculty of Chemistry, University of Sofia, Sofia 1126, Bulgaria; and † Protein Array Project, ERATO, JRDC, 5-9-1 Tokodai, Tsukuba, 300-26 Japan*

Received November 1, 1993; accepted March 8, 1994

In this article we study theoretically the capillary meniscus interaction between a floating submillimeter particle (attached to a fluid interface) and a vertical wall. It is shown that along with the particle weight and the upthrust, there is another force exerted on the particle which is caused by the deformation of the liquid meniscus. The latter we call "capillary image force" because of its similarity to the known image forces in electrostatics. In particular, the capillary image force can be both attractive and repulsive, depending on the specific boundary conditions at the three-phase contact line on the wall surface. Analytical expressions for the capillary interaction energy and force are derived by means of two alternative approaches and the agreement between them is very good. The theory predicts that under certain conditions the energy of interaction between the particle and the wall acquires a minimum; i.e., a stable equilibrium position of the particle at a finite separation from the wall should be observed. This prediction is experimentally proven in the second part of the study.

1. INTRODUCTION

The lateral capillary forces between particles, which are floating attached to the interface between two phases, usually cause interparticle attraction and formation of two-dimensional aggregates. These forces were studied experimentally by Hinsch (1) and Camoin *et al.* (2) and were utilized in some extraction and separation techniques (3, 4). A new interest in the capillary interactions has been aroused by the experimental findings that they can bring about the formation of two-dimensional arrays from submicron particles and even protein macromolecules (5–7).

The lateral capillary forces are due to the overlap of the menisci formed around each of the floating particles. Hence, the main problem in the theory of these forces is the calculation of the shape of the fluid interface, which is determined by the shape, weight, and contact angles of the particles. Gifford and Scriven (8) studied numerically the interaction between two identical horizontal floating cylinders. Nicolson (9) and Chan *et al.* (10) derived analytical expressions for floating spheres and horizontal cylinders by using a superposition approximation. More accurate expressions for the system of two floating spheres were derived in Ref. (11), where a solution of the Laplace equation of capillarity in bipolar coordinates was used.

The capillary interaction between two partially immersed spheres on substrate, or two vertical cylinders, was studied theoretically in Refs. (12, 13) and experimentally in Ref. (14). It is worthwhile noting that lateral capillary forces appear also between particles confined in a thin liquid film, when the disjoining pressure of the film also affects the shape of the interfaces (12, 15).

Closely related to the present study is the theoretical investigation (16) of the particle–wall interaction in the case of a sphere, which is partially immersed in a liquid layer on substrate in the neighborhood of a vertical wall. In Ref. (16) the liquid layer was assumed to be almost plane-parallel with thickness smaller than the particle diameter. (Otherwise, if the thickness is greater and the particle is entirely immersed inside the liquid layer, the capillary force will disappear.) It was established in Ref. (16) that the meniscus between the particle and the wall (if the wall contact angle is 90°) has the same shape as the meniscus between two identical particles, each of them being the *mirror image* of the other one with respect to the wall surface. For this reason, in such a case the capillary interaction between the particle and the wall is the same as that between the particle and its mirror image. In this aspect there is some analogy with the image forces in electrostatics.

The particle (sphere on substrate) studied in Ref. (16) is not allowed to move in a vertical direction. Our aim in the present study is to extend and generalize the analysis in Ref. (16) in the following aspects:

(i) To consider floating spherical particles attached to an inclined fluid meniscus at a vertical wall. In this case there is no restriction on the vertical movement of the particle,

[1] To whom correspondence should be addressed.

0021-9797/94 $6.00

and the capillary image force interferes with the gravitational and buoyancy forces exerted on the particle.

(*ii*) The analogy with electrostatics suggests that not only attractive, but also repulsive image forces could exist. One of our purposes here is to specify the conditions under which *repulsive* image forces can appear and to investigate them in detail together with the attractive image forces (the latter being similar to those studied in Ref. (16)).

(iii) In Ref. (16) only the so called "force approach" to the theory of capillary interactions was applied (see, e.g., Ref. (13)). Below we make use of both the "force approach" and the alternative "energy approach" and compare their predictions.

It should be noted that we restrict our considerations to an equilibrium system. In other words we assume that the projection of the capillary force along the tangent to the liquid meniscus (where the particle is attached) is exactly counterbalanced by some external force. If the external force is removed, the particle will float along the meniscus surface driven by gravity and the capillary image force. However, in such a nonequilibrium situation a viscous flow will appear in the fluid phases. This complicated nonequilibrium (hydrodynamic) problem is out of the scope of the present study.

The article is organized as follows. The next section is devoted to the "pure" capillary image forces, appearing in the special case when the interface at the wall is horizontal in the absence of the floating particles. Section 3 considers the meniscus shape in the more complicated (and realistic) case when an inclined meniscus is formed at the wall. General expressions for the energy of capillary interaction are derived in Section 4. Section 5 is devoted to the alternative "force approach." Finally, numerical results are presented and discussed.

The repulsive capillary image forces, predicted theoretically in the present paper, are observed experimentally, and this is the subject of the second part of this study, Ref. (17).

2. ATTRACTIVE AND REPULSIVE CAPILLARY IMAGE FORCES

Imagine a floating spherical particle in the vicinity of a vertical planar wall. The particle is attached to the interface between two fluid phases, I and II, of mass densities ρ_I and ρ_{II}, respectively. Below we will use indices 1 and 2 to denote properties belonging to the wall and particle, respectively. For example, we denote by ψ_1 and ψ_2 the angles characterizing the meniscus slope at the wall and at the particle contact line (see below for details). The particle can be both heavy ($\psi_2 < 0$) and light ($\psi_2 > 0$, e.g., bubble).

The physical origin of the capillary interaction between a floating particle and a wall lies on the fact that the wall perturbs the interfacial deformation created by the particle. As discussed below, the range of the capillary interaction can be characterized by the so-called capillary length, q^{-1}

$$q \equiv (\Delta\rho g/\gamma)^{1/2}, \quad \Delta\rho \equiv \rho_I - \rho_{II}, \qquad [2.1]$$

where γ is the interfacial tension and g is the gravity acceleration. Thus for a water–gas interface ($\Delta\rho = 1$ g/cm^3, $\gamma = 72$ mN/m) one has $q^{-1} = 2.7$ mm.

We assume that far away from the particle and the wall, the interface is flat and horizontal. The coordinate plane xy is chosen to coincide with the plane of this horizontal interface. The vertical plane xz is perpendicular to the wall and passes through the particle center. Let $z = \zeta(x, y)$ be the equation describing the shape of the meniscus surface. The explicit form of $\zeta(x, y)$ can be determined by solving the Laplace equation of capillarity (18)

$$\nabla_{II}\cdot\left[\frac{\nabla_{II}\zeta}{(1 + |\nabla_{II}\zeta|^2)^{1/2}}\right] = q^2\zeta, \ \nabla_{II} \equiv \left(\frac{\partial}{\partial x}, \frac{\partial}{\partial y}\right), \qquad [2.2]$$

under appropriate boundary conditions. The two-dimensional divergence in Eq. [2.2] represents in fact the mean curvature of the interface. For small interfacial slope,

$$|\nabla_{II}\zeta|^2 \ll 1, \qquad [2.3]$$

Eq. [2.2] can be linearized

$$\nabla_{II}^2\zeta = q^2\zeta \qquad [2.4]$$

It is instructive first to consider the simpler case, when the contact angle at the wall is $\alpha_1 = \pi/2$; hence $\psi_1 = \pi/2 - \alpha_1 = 0$. In this case the meniscus would be flat ($\zeta \equiv 0$) if the floating particle is removed. We denote by $\zeta_0(x, y)$ the meniscus shape in the presence of the particle. Since $\psi_1 = 0$ the function $\zeta_0(x, y)$ must satisfy the following boundary condition at the wall surface

$$\left.\frac{\partial\zeta_0}{\partial x}\right|_{x=0} = 0. \qquad [2.5]$$

By using considerations for symmetry one can realize that in view of Eq. [2.5], the function $\zeta_0(x, y)$ would be the same, if (instead of a wall at a distance s from the particle) one has a second particle (*image*) floating at a distance $2s$ from the original one—see Fig. 1a. The image must be identical to the original particle with respect to the size, weight, and contact angle. In other words, the spherical particle and its image ought to have identical "capillary charges," Q_2, defined (11)

$$Q_2 = r_2 \sin\psi_2. \qquad [2.6]$$

Here r_2 is the radius of the three-phase contact line at the particle surface. The notion of capillary charge, introduced in Ref. (11), originates from the fact that the lateral capillary

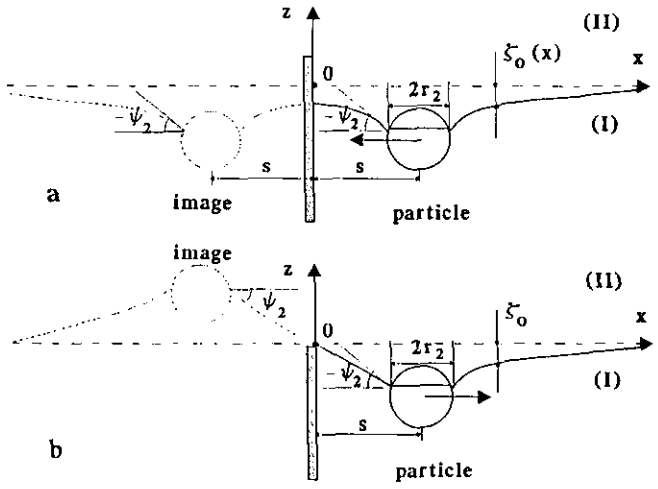

FIG. 1. Sketch of a floating particle in the vicinity of a vertical wall. r_2 is the radius of the three-phase contact line of the particle and ψ_2 is the meniscus slope angle at the particle contact line: (a) fixed contact angle at the wall (90°), corresponding to attractive capillary image forces, and (b) fixed contact line at the wall, leading to repulsive image force. $\zeta_0(x, y)$ describes the meniscus shape.

force, F, between two floating submillimeter particles, obeys an asymptotic law representing a two-dimensional counterpart of Coulomb's law (11):

$$F = -2\pi\gamma \frac{Q_1 Q_2}{L} \quad r_2 \ll L \ll q^{-1}. \qquad [2.7]$$

Here $Q_k = r_k \sin \varphi_k$ ($k = 1, 2$) are the capillary charges of the particles and L is the distance between them (in our case $L = 2s$ and Q_1 accounts for the image—see Fig. 1). In the particular case shown in Fig. 1a, $\varphi_1 = \varphi_2 = \psi_2$, whereas in Fig. 1b, $-\varphi_1 = \varphi_2 = \psi_2$. In Eq. [2.7] F is negative (positive) when the force is attractive (repulsive). In particular, F corresponds to attraction when $Q_1 Q_2 > 0$.

For two identical floating particles the lateral capillary force is always attractive (11). Hence, the particle and its image, depicted in Fig. 1a, will attract each other; i.e., in reality the wall will attract the floating particle. Moreover, the resulting image force will obey Eq. [2.7] (in the range of its validity) with $Q_1 = Q_2$. (Equations [2.10] and [2.15] below provide more general expressions for F.)

In some aspects the capillary image forces resemble the *electrostatic* image forces, appearing when an electric charge, imbedded in a medium of dielectric permittivity ϵ_1, is located in the neighborhood of a boundary with a second medium of permittivity ϵ_2. The electrostatic image forces can be both attractive and repulsive depending on whether $\epsilon_2 > \epsilon_1$ or $\epsilon_2 < \epsilon_1$—see, e.g., Ref. (19). The difference $(\epsilon_2 - \epsilon_1)$ enters the expression for the force under the electrostatic boundary condition at the interface.

As mentioned above, the boundary condition, Eq. [2.5], leads to *attractive* capillary image forces, which was noted in Ref. (16). The analogy between the electric and capillary image forces suggests one to look for some boundary condition, which can lead to repulsive image forces. Such a boundary condition can be

$$\zeta_0|_{x=0} = 0, \qquad [2.8]$$

which represents a requirement for a zero elevation of the contact line at the wall. This can be realized in practice if the contact line is attached to the edge of a vertical plate, as shown in Fig. 1b, or to the boundary between hydrophilic and hydrophobic domains on the surface of the wall. By using again considerations for symmetry, one can realize that in view of Eq. [2.8] and Fig. 1b, the function $\zeta_0(x, y)$ would be the same if (instead of the wall at distance s from the particle) one has a second particle (image) of the *opposite* capillary charge ($Q_1 = -Q_2$) at a distance $2s$ from the original particle. In such case the lateral capillary force is repulsive (11); i.e., in reality the wall will repel the floating particle.

In summary, the capillary image force can be monotonic attraction or repulsion for all values of the particle–wall separation, s, depending on whether the boundary condition at the wall is given by Eq. [2.5] or [2.8]. In the special cases discussed above the particle–wall interaction is equivalent to the capillary interaction of the particle with its image of the same or opposite capillary charge—cf. Figs. 1a and 1b. Then one can use the expressions for the energy, ΔW, and force, F, of capillary interaction derived in our previous paper, Ref. (11). In particular, from Eqs. [6.7] and [7.7] in Ref. (11) one obtains

$$\Delta W = -\pi\gamma(Q_2 h_2 - Q_{2\infty} h_{2\infty})[1 + O(q^2 R_2^2)] \qquad [2.9]$$

$$F \equiv -\frac{d\Delta W}{ds} = \pi\gamma Q_2 \frac{dh_2}{ds}[1 + O(q^2 R_2^2)], \qquad [2.10]$$

where ΔW is the capillary interaction energy in the real system (on the right of the wall surface—Figs. 1a and 1b), so ΔW is half of the energy as given by Eq. [6.7] in Ref. (11);

$$h_2 \equiv \frac{1}{2\pi r_2} \oint_{C_2} \zeta dl \qquad [2.11]$$

is the mean elevation of the particle contact line with respect to the horizontal surface $z = 0$; C_2 is a contour representing the orthogonal projection of the particle contact line on the plane xy; R_2 is the particle radius; and the subscript ∞ denotes the value of the respective quantity at infinite particle–wall separation ($s \to \infty$). The capillary charge in this case can be estimated by means of the expression (Eq. [6.13] in Ref. 11),

$$Q_2 \approx Q_{2\infty} = \tfrac{1}{6} q^2 R_2^3 (2 - 4D_2 + 3\cos\alpha_2 - \cos^3\alpha_2) \times [1 + O(qR_2)], \qquad [2.12]$$

where

$$D_2 \equiv (\rho_2 - \rho_{II})/(\rho_I - \rho_{II}), \qquad [2.13]$$

with ρ_2 being the particle mass density. The asymptotic forms of Eqs. [2.9] and [2.10] for not-too-small separations read (11)

$$\Delta W = \pi\gamma(-1)^{\lambda}Q_2^2K_0(2qs) \times [1 + O(q^2R_2^2)],\ r_2 \ll s \qquad [2.14]$$

$$F = 2\pi\gamma(-1)^{\lambda}Q_2^2qK_1(2qs) \times [1 + O(q^2R_2^2)],\ r_2 \ll s, \qquad [2.15]$$

where K_0 and K_1 are modified Bessel functions and

$$\lambda = \begin{cases} 1 \text{ for fixed contact angle at the wall;} \\ 0 \text{ for fixed contact line at the wall.} \end{cases} \qquad [2.16]$$

Since $K_1(x) \approx 1/x$ for $x \ll 1$ (20), one can check that Eq. [2.7] is a corollary of Eq. [2.15] with $Q_1 = (-1)^{\lambda+1}Q_2$. Note that $K_1(2qs)$ decays exponentially for $s \to \infty$ with a decay length $(2q)^{-1}$, i.e., the capillary length q^{-1} really determines the range of the capillary image forces, as mentioned in advance.

The above considerations may give the impression that the theoretical treatment of the capillary image forces reduces to a mere application of some equations for two floating particles (the original particle and its image) derived elsewhere (10, 11). However, the situation discussed above corresponds to the very particular case when the fluid interface becomes flat if the floating particle is removed. For the sake of convenience we will call the forces in this special case "pure image forces."

In reality, an inclined meniscus is formed in a neighborhood of a wall, even in the absence of any floating particles. In this case the capillary image force interferes with the gravity force which tends to "slip" the particle along the meniscus created by the wall. The remaining part of the paper is devoted to derivation of expressions for ΔW and F in this more general case.

3. INCLINED MENISCUS AT THE WALL

(a) Configuration of the System

Figure 2 shows a typical configuration: a capillary meniscus formed at a planar vertical wall (the plane yz) in the presence of a heavy particle. In the absence of a particle the meniscus shape is determined by the equation $z = \zeta_1(x)$—the dashed line in Fig. 2a. We restrict our considerations to the case of a small meniscus slope:

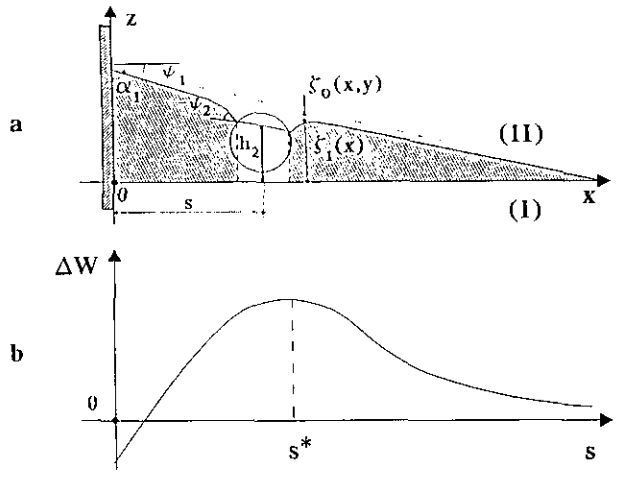

FIG. 2. Sketch of the capillary meniscus (a) around a heavy particle floating in the vicinity of a vertical planar wall of fixed three-phase contact angle ($\alpha_1 < 90°$). $\zeta_1(x)$ is the nondisturbed meniscus of the wall with $\zeta_0(x, y)$ being the meniscus perturbation created by the particle. (b) Typical curve of capillary interaction energy, ΔW, vs separation, s, for such a configuration.

$$\left|\frac{d\zeta_1}{dx}\right|^2 \ll 1. \qquad [3.1]$$

In fact, this is the nontrivial case corresponding to an interplay of gravity (weight plus upthrust) and capillary image forces. (Indeed, if the meniscus slope is larger, the capillary image force becomes negligible compared to the gravity force and the problem becomes trivial.)

The corresponding energy of capillary interaction, ΔW, is depicted qualitatively in Fig. 2b. As far as we consider the case of a mobile contact line, but of a fixed contact angle at the wall, the "pure" capillary image force is attractive. One can expect that the image force will prevail at small separations, s, if the particle is not too small. On the contrary, at larger separations the image force decays faster and the gravity will tend to bring the particle away from the wall. Hence, the energy ΔW will exhibit a maximum at some separation $s = s^*$, which corresponds to an unstable equilibrium position of the particle—see Fig. 2b.

If $\alpha_1 > 90°$ ($\psi_1 < 0$) the plot of ΔW vs s will be a monotonically increasing curve for a heavy particle ($Q_2 < 0$), because in this case both the capillary image force and gravity will tend to bring the particle closer to the wall.

In the case of a light particle ($Q_2 > 0$, e.g., bubble) similar considerations lead to the conclusion that $\Delta W(s)$ will correspond to a monotonic "attraction" when $\psi_1 > 0$ ($\alpha_1 < 90°$) and to a curve with a maximum, like that in Fig. 2b, when $\psi_1 < 0$ ($\alpha_1 > 90°$).

Physically more interesting is the case, depicted in Fig. 3, corresponding to a contact line, whose position is fixed at the wall by attachment to an edge or to the boundary between hydrophilic and hydrophobic domains on the surface of the

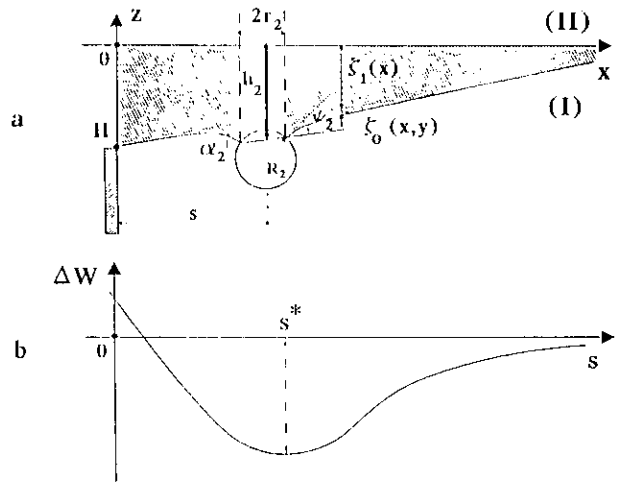

FIG. 3. Sketch of the capillary meniscus (a) around a heavy particle of radius R_2 floating in the vicinity of a vertical plate whose three-phase contact line is fixed at the edge. H is the maximum elevation of the liquid interface with respect to the wall contact line. (b) The curve representing the capillary interaction energy, ΔW, vs separation, s, exhibits a minimum for this configuration.

wall. In this case the pure capillary image force is repulsive. Let H be the z coordinate of the contact line at the wall. When $H < 0$, as in Fig. 3a, the gravity will tend to bring a heavy particle ($Q_2 < 0$) closer to the wall; however, at small s the repulsive image force will oppose the approach of the floating particle to the wall. Hence, at some separation $s = s^*$ the capillary image force can counterbalance the gravity and the particle will have an equilibrium position, corresponding to a minimum of ΔW as shown in Fig. 3b. Similar dependence of ΔW vs s appears when $H > 0$ and the particle is light ($Q_2 > 0$).

The presence of a minimum in the plot of ΔW vs s provides a possibility to determine the equilibrium separation, s^*, between the particle and the wall and to verify the theoretical predictions against equilibrium experimental data. The particle–wall configurations ($H < 0$, $Q_2 > 0$) and ($H > 0$, $Q_2 < 0$) correspond to monotonous repulsion between the particle and the wall.

Below we focus our attention on the *quantitative* study of the theoretical curves $\Delta W(s)$, which is a prerequisite for the interpretation of experimental data.

(b) Expressions for the Shape of the Particle Contact Line

Here we follow a general theoretical approach, which is applicable to all configurations discussed in the previous subsection. The only limitation is that we suppose small meniscus slope, i.e., that Eq. [2.3] holds. This condition is satisfied with submillimeter particles and with menisci on the wall satisfying Eq. [3.1].

Since for a small meniscus slope the Laplace equation of capillarity is linear, i.e., $\zeta(x, y)$ satisfies Eq. [2.4], one can seek the solution as a superposition of the meniscus $\zeta_1(x)$, which is formed in the absence of a floating particle, and the interfacial deformation, $\zeta_0(x, y)$, created by the particle,

$$\zeta(x, y) = \zeta_0(x, y) + \zeta_1(x). \qquad [3.2]$$

As $\zeta_1(x)$ by definition satisfies Eq. [2.4] one has

$$\frac{d^2\zeta_1}{dx^2} = q^2\zeta_1. \qquad [3.3]$$

Then from Eqs. [2.4], [3.2], and [3.3] one obtains

$$\frac{\partial^2\zeta_0}{\partial x^2} + \frac{\partial^2\zeta_0}{\partial y^2} = q^2\zeta_0. \qquad [3.4]$$

In the case of a fixed contact *angle* at the wall, the boundary conditions at the wall surface are

$$\left.\frac{d\zeta_1}{dx}\right|_{x=0} = -\tan\psi_1 = \text{const}; \quad \left.\frac{\partial\zeta_0}{\partial x}\right|_{x=0} = 0. \qquad [3.5]$$

(For the boundary condition at the particle surface, see Eq. [3.46] below.) Since ζ_1 should vanish at $x \to \infty$, from Eqs. [3.3] and [3.5] one derives

$$\zeta_1(x) = q^{-1}\tan\psi_1 e^{-qx} \quad \text{(fixed contact angle)}. \qquad [3.6]$$

In the case of fixed contact *line* at the wall, the following boundary conditions are applicable at the wall:

$$\zeta_1|_{x=0} = H = \text{const}; \quad \zeta_0|_{x=0} = 0. \qquad [3.7]$$

The counterpart of Eq. [3.6], stemming from Eqs. [3.3] and [3.7], reads

$$\zeta_1(x) = He^{-qx} \quad \text{(fixed contact line)}. \qquad [3.8]$$

A comparison between Eqs. [2.5] and [3.5] (or between Eqs. [2.8] and [3.7]) shows that ζ_0 in fact represents the meniscus shape, corresponding to the pure capillary image force considered in Section 2. Hence the meniscus shape determined by $\zeta_0(x, y)$ is the same as that in the case of two floating particles (the original particle and its image) separated at a center-to-center distance $2s$.

In our previous studies (12, 13) we solved Eq. [3.4] in bipolar coordinates for not-too-large interparticle separations, $(qs)^2 \ll 1$. The presence of a small parameter in the theory allows us to use the method of the matched asymptotic expansions in its simpler version: the procedure of Prandtl for matching the zeroth-order "outer" and "inner" expansions (25). This method provides a scheme which allows us to find a uniformly valid (approximate) expression when the

outer and inner asymptotes are known (25). In the present study we obtain more general compound asymptotic expressions for the shape of the particle contact line $\zeta_0|_{x,y\in C_2}$ which are uniformly valid at arbitrary separation.

For the case of a *fixed contact angle at the wall* and small separations we can use the equation for the particle contact line for two *identical* particles, derived in Ref. (12):

$$\zeta_0^{\text{in}}(\sigma) = Q_2[\ln 2(\cosh\tau_2 - \cos\sigma) - 2\ln(\gamma_e qa)], (qa)^2 \ll 1. \quad [3.9]$$

The superscript "in" denotes the inner asymptotic region, $(qa)^2 \ll 1$, corresponding to a close approach of the particle to the wall, compared with the capillary length, q^{-1}. In Eq. [3.9] $\gamma_e = 1.781071\cdots$ is the constant of Euler–Masceroni and (σ, τ) are bipolar coordinates in the plane xy (see, e.g., Ref. (21)),

$$x = \frac{a\sinh\tau}{\cosh\tau - \cos\sigma}, \quad y = \frac{a\sin\sigma}{\cosh\tau - \cos\sigma} \quad [3.10]$$
$$-\pi \leqslant \sigma \leqslant \pi, \qquad 0 \leqslant \tau < \infty,$$

where a is connected with the particle–wall separation s:

$$a = \sqrt{s^2 - r_2^2}. \quad [3.11]$$

The coordinate lines of the bipolar coordinates are circumferences, as illustrated in Fig. 4. Here $\tau = \tau_2$ is the τ coordinate of the horizontal projection of the particle contact line

$$\cosh\tau_2 = \frac{s}{r_2}, \quad \sinh\tau_2 = \frac{a}{r_2}. \quad [3.12]$$

Using Eq. [3.12] one can express τ_2 in two alternative forms:

$$\tau_2 = \ln(a/r_2 + \sqrt{a^2/r_2^2 + 1}) = \ln(s/r_2 + \sqrt{s^2/r_2^2 - 1}). \quad [3.13]$$

By means of Eq. [3.13] we bring Eq. [3.9] into the form:

$$\zeta_0^{\text{in}} = Q_2\ln\frac{2}{\gamma_e qr_2} + Q_2\ln\frac{2}{\gamma_e 2qa^2/(s - r_2\cos\sigma)}. \quad [3.14]$$

For large separations, $(qa)^2 \geqslant 1$, one can use the superposition approximation of Nicolson (9), representing the meniscus shape around a couple of particles as a superposition of the deformations, created by two separate single particles. Since the meniscus around a single particle is described by the equation $z(r) = Q_2K_0(qr)$, derived long ago by Derjaguin (22), for the particle contact line we obtain

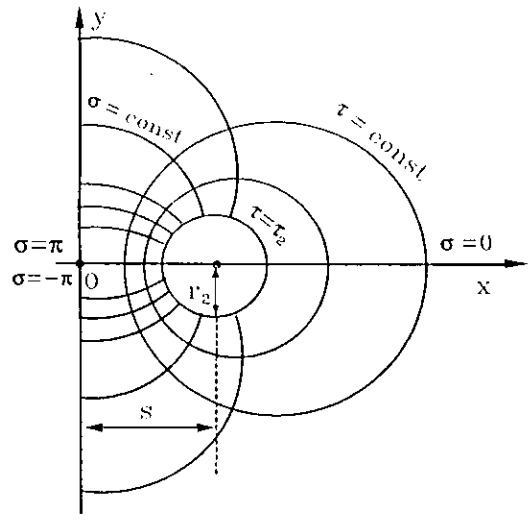

FIG. 4. Bicylindrical coordinates (σ, τ) in the plane xy. The circumference of radius r_2, corresponding to the line $\tau = \tau_2 = \text{const}$, represents the projection of the particle contact line.

$$\zeta_0^{\text{out}}(\sigma) = Q_2K_0(qr_{\text{r}}) \pm Q_2K_0(qr_{\text{l}}), (qs)^2 \geqslant 1, \quad [3.15]$$

where the superscript "out" denotes the fact that the expression for $\zeta_0(\sigma)$, derived by means of the superposition approximation, is correct in the outer asymptotic region of not-too-small interparticle separation, $(qs)^2 \gg 1$; the signs "+" and "−" refer to fixed contact angle and line at the wall, respectively. The indices "l" and "r" denote the left- and right-hand side particles, in particular

$$r_{\text{l}}^2 = (x + s)^2 + y^2, \; r_{\text{r}}^2 = (x - s)^2 + y^2. \quad [3.16]$$

On the other hand, for $(qa)^2 \geqslant 1$ and submillimeter particles ($(qr_2)^2 \ll 1$), $a \approx s$ (cf. Eq. [3.11]) and instead of Eq. [3.16] one can write

$$r_{\text{l}}^2 = (x + a)^2 + y^2, \; r_{\text{r}}^2 = (x - a)^2 + y^2. \quad [3.17]$$

In particular, at the particle contact line $(x, y \in C_2)$, by using Eqs. [3.10]–[3.12] one can transform Eqs. [3.17] to read

$$r_{\text{l}}^2 = \frac{2a^2(s + a)}{s - r_2\cos\sigma}, \quad r_{\text{r}}^2 = \frac{2a^2(s - a)}{s - r_2\cos\sigma}. \quad [3.18]$$

Having in mind the asymptotic expansion

$$K_0(x) = \ln\frac{2}{\gamma_e x} + O(x\ln x), \quad x \ll 1, \quad [3.19]$$

the inner asymptotics (that for $a \to 0$) of Eq. [3.15] read

$$(\zeta_0^{\text{out}})^{\text{in}} \approx Q_2\left[\ln\frac{2}{\gamma_e qr_{\text{r}}} \pm \ln\frac{2}{\gamma_e qr_{\text{l}}}\right]. \quad [3.20]$$

The substitution of Eq. [3.18] into [3.20] (with "+") after some algebra gives exactly Eq. [3.14] without any approximations, i.e.,

$$(\zeta_0^{\text{out}})^{\text{in}} \equiv \zeta_0^{\text{in}}, \qquad [3.21]$$

but only if one uses Eq. [3.17] instead of Eq. [3.16]. Then if in accordance with Eq. [3.19] we return back to K_0 function in Eq. [3.14], we obtain a "compound" expression for $\zeta_0(\sigma)$, which for small separations reduces to ζ_0^{in} (Eq. [3.14]) and for large separations reduces to ζ_0^{out} (Eq. [3.15]):

$$\zeta_0(\sigma) = h_{2\infty} + Q_2 K_0\left(\frac{2qa^2}{s - r_2\cos\sigma}\right),$$

(fixed contact angle) [3.22]

and

$$h_{2\infty} \equiv Q_2 \ln\frac{2}{\gamma_e q r_2}. \qquad [3.23]$$

As shown by Derjaguin (22) $h_{2\infty}$ is the elevation of the contact line for a single particle.

In the case of a *fixed contact line at the wall* we have to use an expression for the shape of the particle contact line for two particles of opposite capillary charge ($Q_1 = -Q_2$). The inner asymptotics of this expression can be obtained by setting $Q_1 = -Q_2$ in Eq. [2.39] of Ref. (13) (with $k = 1, 2$); the result for $(qa)^2 \ll 1$ reads

$$\zeta_0^{\text{in}}(\sigma) = Q_2\tilde{\tau}_2(\sigma), \quad (qa)^2 \ll 1, \qquad [3.24]$$

where

$$\tilde{\tau}_2(\sigma) \equiv \tau_2 + 2\sum_{n=1}^{\infty}\frac{1}{n}\tanh n\tau_2 e^{-n\tau_2}\cos n\sigma. \qquad [3.25]$$

On the other hand, the substitution of Eq. [3.18] into the superposition approximation, Eq. [3.20] (with "−"), yields

$$(\zeta_0^{\text{out}})^{\text{in}} = Q_2\ln\frac{r_1}{r_r} = Q_2\ln\left(\frac{s}{r_2} + \frac{a}{r_2}\right) = Q_2\tau_2. \qquad [3.26]$$

Moreover, since for large separations $\tilde{\tau}_2 \to \tau_2$, Eqs. [3.24] and [3.26] yield

$$(\zeta_0^{\text{out}})^{\text{in}} = (\zeta_0^{\text{in}})^{\text{out}}, \qquad [3.27]$$

as required by the method of the matched asymptotic expansions (25). Similarly to Eq. [3.20] one can rewrite Eq. [3.24] in the form

$$\zeta_0^{\text{in}} = Q_2\ln\frac{2}{\gamma_e q r_2} - Q_2\ln\frac{2}{\gamma_e q r_2 e^{\tilde{\tau}_2}}. \qquad [3.28]$$

Then in accordance with Eq. [3.19] we return back to Bessel function, K_0, in Eq. [3.28]. Thus we construct a compound solution, which is uniformly valid for the all range of separations:

$$\zeta_0(\sigma) = h_{2\infty} - Q_2 K_0(qr_2 e^{\tilde{\tau}_2(\sigma)}),$$

(fixed contact line). [3.29]

One can verify that for small separations, $(qa)^2 \ll 1$, Eq. [3.29] reduces to Eq. [3.24], and for large separations, $(qa)^2 \gg 1$, asymptotically tends toward the superposition approximation, Eq. [3.15] with "−."

(c) Elevation of the Particle Contact Line

The calculation of $h_2 = h_2(s)$ is an auxiliary problem toward our final goal: to derive an analytical expression for the capillary interaction energy $\Delta W(s)$.

(i) Fixed contact angle at the wall. As we consider submillimeter floating particles ($q^2R_2^2 \ll 1$) at a small meniscus slope, from Eqs. [2.11], [3.2], and [3.6] we obtain

$$h_2 = q^{-1}\tan\psi_1 e^{-qs} + h_{20};\ h_{20} \equiv \frac{1}{2\pi r_2}\oint_{C_2}\zeta_0 dl. \qquad [3.30]$$

In the inner region, $(qa)^2 \ll 1$, the following expression for the mean capillary elevation was derived in Ref. (12) for two identical particles,

$$h_{20}^{\text{in}} = Q_2\left[\tau_2 + 2\ln\frac{1 - \exp(-2\tau_2)}{\gamma_e qa}\right],\ (qa)^2 \ll 1, \qquad [3.31]$$

where a and τ_2 are defined by means of Eqs. [3.11] and [3.13] above.

For $(qa)^2 \geqslant 1$ (in the outer region) one can use the superposition approximation of Nicolson (9) to derive

$$h_{20}^{\text{out}} = h_{2\infty} + Q_2 K_0(2qs), \quad (qa)^2 \geqslant 1, \qquad [3.32]$$

where, as usual, $h_{2\infty}$ is the elevation of the contact line for a single particle and $Q_2K_0(2qs)$ is the elevation at a distance $2s$ from another single particle (the image).

Below we proceed with the derivation of a generalization of Eq. [3.31] which expresses h_{20} for all values of qa. By using Eq. [3.13], after some transformations (without any approximations), one can rewrite Eq. [3.31] in the form

$$h_{20}^{\text{in}} = Q_2\ln\frac{2}{\gamma_e qr_2} + Q_2\ln\frac{2}{\gamma_e q(s+a)},\ (qa)^2 \ll 1. \qquad [3.33]$$

Taking into account the asymptotics of the Bessel function, K_0, Eq. [3.19], and Eq. [3.23], one obtains a compound expression for h_{20}:

$$h_{20} = h_{2\infty} + Q_2 K_0(q(s + a)). \qquad [3.34]$$

One can check that Eqs. [3.31] and [3.32] are limiting cases of Eq. [3.34]. Finally, the substitution of Eq. [3.34] into Eq. [3.30] yields

$$h_2 = q^{-1}\tan\psi_1 e^{-qs} + h_{2\infty} + Q_2 K_0(q(s + a)). \qquad [3.35]$$

We recall that Eq. [3.35] holds in the case of a fixed contact angle at the wall.

(ii) Fixed contact line at the wall. By means of Eqs. [2.11], [3.2], and [3.8], one obtains an analogue of Eq. [3.30]:

$$h_2 = He^{-qs} + h_{20}, \quad h_{20} \equiv \frac{1}{2\pi r_2}\oint_{C_2} \zeta_0 dl. \qquad [3.36]$$

By substituting ζ_0 from Eq. [3.24] into Eq. [3.36] and carrying out the integration one derives

$$h_{20}^{\text{in}} = Q_2\tau_2^*, \quad (qa)^2 \ll 1, \qquad [3.37]$$

where

$$\tau_2^* \equiv \tau_2 + \sum_{n=1}^{\infty}\frac{2}{n}e^{-2n\tau_2}\tanh n\tau_2 \qquad [3.38]$$

Here τ_2 is given by Eq. [3.13]. For $(qa)^2 \geqslant 1$ (that is for $(qs)^2 \geqslant 1$) by using the superposition approximation one obtains an analogue of Eq. [3.32],

$$h_{20}^{\text{out}} = h_{2\infty} - Q_2 K_0(2qs), \quad (qa)^2 \geqslant 1, \qquad [3.39]$$

where $h_{2\infty}$ is determined by Eq. [3.23].

Equation [3.37] can be rewritten in the form

$$h_{20}^{\text{in}} = Q_2\ln\frac{2}{\gamma_e qr_2} - Q_2\ln\frac{2}{\gamma_e qr_2 e^{\tau_2^*}}, \; (qa)^2 \ll 1. \qquad [3.40]$$

Returning back to the Bessel function, K_0, by means of Eq. [3.19] one constructs the compound expression for h_{20}, which is uniformly valid for arbitrary separations, qs:

$$h_{20} = h_{2\infty} - Q_2 K_0(qr_2 e^{\tau_2^*}). \qquad [3.41]$$

It can be proven that Eqs. [3.37] and [3.39] are limiting cases of Eq. [3.41]. Substituting Eq. [3.41] into Eq. [3.36] we finally obtain

$$h_2 = He^{-qs} + h_{2\infty} - Q_2 K_0(qr_2 e^{\tau_2^*}). \qquad [3.42]$$

Equation [3.42] enables us to calculate the particle contact line elevation in the case of fixed contact line at the wall.

(d) The Normal Force Balance and the Capillary Charge

Since a floating particle moves *tangentially* to the inclined liquid meniscus under the combined action of gravity and capillary image forces, it is natural to suppose that the net force exerted on the particle has zero projection along the *normal* $\mathbf{n}$ to the meniscus surface $z = \zeta_1(x)$. This is analogous to the case of a slipping solid body on an inclined solid plane, when the normal projection of the weight of the body is counterbalanced by the bearing reaction of the substrate. (The difference between the cases of solid and liquid substrates is only in the fact that the deformation of the solid is negligible, whereas the deformation of the liquid surface is significant and should be taken into account.) Then the balance of the forces along the normal $\mathbf{n}$ reads

$$(\mathbf{F}^{(w)} + \mathbf{F}^{(p)})\cdot\mathbf{n} = -\mathbf{F}^{(\gamma)}\cdot\mathbf{n} = 2\pi r_2\gamma\sin\psi_2, \qquad [3.43]$$

where $\mathbf{F}^{(w)}$, $\mathbf{F}^{(\gamma)}$, and $\mathbf{F}^{(p)}$ are the forces due to the particle weight, meniscus interfacial tension, γ, and the hydrostatic pressure (buoyancy), respectively. The interfacial tension γ acts tangentially to the liquid meniscus, which meets the plane of the contact line at angle ψ_2. (As discussed in Ref. (12) the contact line is not exactly a planar circumference; however, the deviation from planarity is negligible when Eq. [2.3] holds.) Using some geometrical considerations one can relate ψ_2 with the three-phase contact angle α_2,

$$b_2 = R_2[1 + \cos(\alpha_2 + \psi_2)], \qquad [3.44]$$

where b_2 is the depth of immersion of the spherical particle inside the lower fluid (phase I)—see Fig. 3a. For a spherical particle of radius R_2 the depth of immersion b_2 determines the contact line radius:

$$r_2 = [b_2(2R_2 - b_2)]^{1/2}. \qquad [3.45]$$

Angle ψ_2 enters in the boundary condition for Eq. [3.4] at the particle contact line (see Ref. (12) for details),

$$\mathbf{e}_\tau\cdot\nabla_{\text{II}}\zeta_0|_{\tau=\tau_2} = (\cosh\tau_2 - \cos\sigma)\frac{1}{a}\frac{\partial\zeta_0}{\partial\tau}\bigg|_{\tau=\tau_2}$$

$$= \sin\psi_2 = \text{const}, \qquad [3.46]$$

where $\mathbf{e}_\tau$ is the unit vector along the τ lines.

Let $\mathbf{e}_z$ be the unit vector of the z axis and ψ be the running slope angle of the nondisturbed meniscus $\zeta_1(x)$. In keeping with Eq. [3.1] one obtains

$$\mathbf{e}_z \cdot \mathbf{n} = \cos\psi = 1 - \frac{1}{2}\left(\frac{d\zeta_1}{dx}\right)^2 \approx 1. \qquad [3.47]$$

Then one can write approximately

$$(\mathbf{F}^{(w)} + \mathbf{F}^{(p)}) \cdot \mathbf{n} = F_z^{(w)} + F_z^{(p)}. \qquad [3.48]$$

Eqs. [2.6], [3.43], and [3.48] yield

$$Q_2 = (F_z^{(w)} + F_z^{(p)})/2\pi\gamma. \qquad [3.49]$$

By using an available expression for $(F_z^{(w)} + F_z^{(p)})$, Eq. [32] in Ref. (23), one can transform Eq. [3.49] to read (11)

$$Q_2 = \tfrac{1}{6}q^2[(3R_2 - b_2)b_2^2 - 4D_2R_2^3 - 3r_2^2h_2]. \qquad [3.50]$$

Formally Eq. [3.50] coincides with Eq. [7.2] in Ref. (11). However, h_2 on the right-hand side of Eq. [3.50] now contains a contribution from both ζ_0 and ζ_1 (cf. Eqs. [2.11] and [3.2]), whereas ζ_1 is identically zero in Ref. (11). In the configurations depicted in Figs. 2 and 3 one can have $|\zeta_1| \gg |\zeta_0|$; hence in the present case the contribution of h_2 in Eq. [3.50] should not be neglected (as we did in Ref. (11) to derive Eq. [2.12], the latter being applicable for calculation of Q_2 only when $|\zeta_1| \ll |\zeta_0|$).

4. ENERGY OF CAPILLARY INTERACTION

According to Eq. [2.2] in Ref. (12) the free energy of the system can be represented as a superposition of gravitational, wetting, and liquid meniscus contributions:

$$W = W_g + W_w + W_m. \qquad [4.1]$$

In our case W will depend on the separation s between the particle and the wall—see Figs. 2 and 3. We call capillary interaction energy the difference:

$$\Delta W(s) = W(s) - W(\infty). \qquad [4.2]$$

A detailed derivation of an expression for ΔW can be found in Ref. (11) for the case of two floating particles. That is why here we focus our attention on some points, which are specific for particle–wall interaction, and will utilize some results from Ref. (11) when this is possible.

Let us start with the free energy of wetting, W_w. When the particle–wall separation, s, is varied, W_w will vary because the contact lines at the particle and wall surfaces can change their positions thus altering the areas wet by phases I and II.

Here we assume that the meniscus surface meets the surface of the *floating particle* at the *equilibrium* contact angle, α_2. Under this condition it is proven in Ref. (11) that the wetting free energy of the particle can be represented in the form

$$W_w^{\text{particle}}(s) = -2\pi\gamma R_2 b_2(s)\cos\alpha_2 + \text{const}, \qquad [4.3]$$

where the additive constant does not depend on s. If one assumes formation of equilibrium contact angle, α_1, at the wall, similar consideration yields

$$W_w^{\text{wall}}(s) = -\gamma\cos\alpha_1 \Delta A_w(s) + \text{const}, \qquad [4.4]$$

where W_w^{wall} is the wetting free energy of the wall and

$$\Delta A_w = \int_{-\infty}^{+\infty} dy\zeta_0(x = 0, y) \qquad [4.5]$$

is the change in the area of the wall surface, which is wetted by phase I, due to the presence of a floating particle in a neighborhood of the wall. It is proven in Appendix I that

$$\Delta A_w = 2\pi Q_2 q^{-1} e^{-qa}. \qquad [4.6]$$

As far as we deal with a vertical wall and small meniscus slope (cf. Eq. [3.1]), one has $\cos\alpha_1 = \sin\psi_1 \approx \tan\psi_1$. Then from Eqs. [4.3] and [4.4] one obtains the free energy of capillary interaction due to wetting:

$$\Delta W_w = -2\pi\gamma(R_2 b_2 \cos\alpha_2 + \lambda Q_2 q^{-1}\tan\psi_1 e^{-qa}) - W_{w\infty}. \qquad [4.7]$$

Here $W_{w\infty}$ equals the sum of the limiting values of the other terms on the right-hand side of Eq. [4.7] for $s \to \infty$, i.e., $\Delta W_w(s \to \infty) = 0$; parameter λ, defined by Eq. [2.16], accounts for the fact that the wetting free energy of the wall does not contribute to ΔW_w when the position of the contact line at the wall is fixed.

Let us proceed with the energy W_m due to the surface free energy of the liquid meniscus (the boundary between the fluid phases I and II—see Figs. 2 and 3). W_m depends upon the particle–wall separation s, because the shape of the meniscus (and hence its area) depends on s. W_m can be represented in the form (12)

$$W_m(s) = \gamma[\Delta A^P(s) - A_2^C(s)] + \text{const}, \qquad [4.8]$$

where the constant does not depend on s. $\Delta A^P(s)$ is the difference between the area of the disturbed meniscus and its othogonal projection on the nondisturbed meniscus, $z = \zeta_1(x)$; A_2^C is the area encircled by the projection of the contact line on the nondisturbed meniscus. $\Delta A^P(s)$ can be presented in the form

$$\Delta A^P = \int_{S_m} [(1 + |\nabla_{II}\zeta|^2)^{1/2} - (1 + |\nabla_{II}\zeta_1|^2)^{1/2}]ds, \qquad [4.9]$$

where S_m denotes the surface outside the hatched areas (the horizontal projections of the wall and the particle contact line) in Fig. 5. Since we deal with a small meniscus slope one obtains (cf. Eqs. [2.3] and [3.2])

$$A_2^C \approx \pi r_2^2 \qquad [4.10]$$

$$\Delta A^P \approx \frac{1}{2}\int_{S_m} [(\nabla_{II}\zeta_0)\cdot\nabla_{II}\zeta_0 + 2(\nabla_{II}\zeta_0)\cdot\nabla_{II}\zeta_1]ds. \qquad [4.11]$$

By using the linearized Laplace equation, Eq. [2.4], one derives

$$(\nabla_{II}\zeta_0)\cdot\nabla_{II}\zeta_k = \nabla_{II}\cdot(\zeta_k\nabla_{II}\zeta_0) - q^2\zeta_0\zeta_k,\ k = 0, 1. \qquad [4.12]$$

Hence

$$\Delta A^P \approx \frac{1}{2}\int_{S_m} \{\nabla_{II}\cdot[(\zeta + \zeta_1)\nabla_{II}\zeta_0] - q^2[\zeta^2 - \zeta_1^2]\}ds. \qquad [4.13]$$

An application of Green's theorem (26) leads to

$$\Delta A^P \equiv \frac{1}{2}J - \frac{1}{2}q^2\int_{S_m}(\zeta^2 - \zeta_1^2)ds, \qquad [4.14]$$

where J denotes

$$J = -\sum_{k=1}^{2}\oint_{C_k} dl(\zeta + \zeta_1)\mu\cdot\nabla_{II}\zeta_0, \qquad [4.15]$$

and C_1 is a "degenerated" contour, representing the horizontal projection of the two sides of the vertical plate (Fig. 5); μ is a running outer unit normal to the respective contour. The dashed rectangular contour in Fig. 5 represents schematically the outer boundary of S_m, which is situated far away from the particle, where $\mu\cdot\nabla_{II}\zeta \to 0$; the latter fact is used to derive Eq. [4.14]. It is proven in Appendix I that

$$J = 2\pi Q_2[h_2 + q^{-1}\tan\psi_1 e^{-qs}],$$

(fixed contact angle at the wall) [4.16]

$$J = 2\pi Q_2[h_2 - He^{-qs}],$$

(fixed contact line at the wall). [4.17]

Let V_m be the volume comprised between S_m and the meniscus surface $z = \zeta(x, y)$—see the hatched area in Figs. 2 and 3. Then

$$\int_{V_m}|z|\,dV = \int_{S_m}ds\int_0^{|\zeta|}zdz = \frac{1}{2}\int_{S_m}\zeta^2 ds. \qquad [4.18]$$

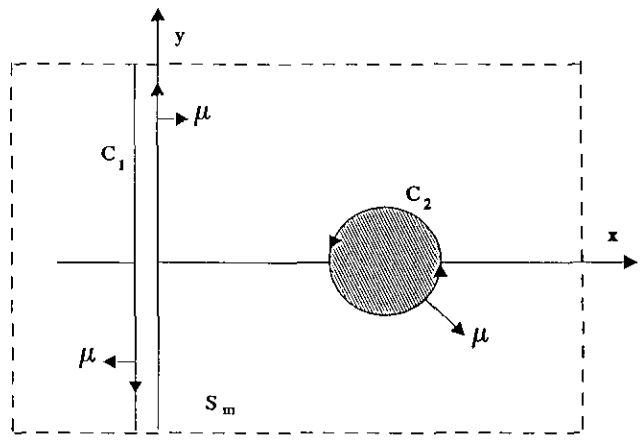

FIG. 5. Projections of the three-phase contact lines of the wall (1) and of the particle (2). The integration area S_m is situated outside of the projection contours C_1 and C_2 with μ being their running outer unit normal.

Besides,

$$\int_{S_m}\zeta_1^2 ds = \text{const} - \int_{A_2^C}\zeta_1^2 ds \approx \text{const} - \pi r_2^2\zeta_1^2(s). \qquad [4.19]$$

The mean value theorem was used to evaluate the integral over A_2^C in Eq. [4.19].

From Eqs. [2.1], [4.8], [4.10], [4.14], [4.18], and [4.19] one obtains the following expression for the capillary interaction energy due to the meniscus deformation:

$$\Delta W_m = \frac{1}{2}\gamma J - \gamma\pi r_2^2 - \frac{1}{2}\pi\gamma(qr_2)^2\zeta_1^2(s) - \Delta\rho g\int_{V_m}|z|dV - W_{m\infty}. \qquad [4.20]$$

The constant $W_{m\infty}$ is chosen in such a way that ΔW_m tends to zero for $s \to \infty$.

Let us proceed with the gravitational contribution, ΔW_g, to ΔW. When the particle–wall separation, s, varies, the meniscus shape (at $x > 0$) changes, which affects the gravitational energy of phases I and II, as well as of the floating particle; the wall is supposed to be immobile. The derivation of an expression for ΔW_g is completely analogous to the respective derivation for two floating particles in Ref. (11). For that reason here we quote only the final result,

$$\Delta W_g = \Delta\tilde{W}_g + \Delta\rho g\int_{V_m}|z|dz - W_{g\infty}, \qquad [4.21]$$

where

$$\Delta\tilde{W}_g = -\pi\gamma\{2Q_2h_2 - q^2[r_2^2(r_2^2 - 2h_2^2)/4 + (4D_2R_2^3 - 3R_2b_2^2 + b_2^3)(R_2 - b_2)/3]\} - \tilde{W}_{g\infty}. \quad [4.22]$$

Equation [4.22] is a particular case of Eq. [4.9] in Ref. (11). The constants $W_{g\infty}$ and $\tilde{W}_{g\infty}$ are determined in such way that for $s \to \infty$ both $\Delta W_{g\infty}$ and $\Delta\tilde{W}_{g\infty}$ tend to zero.

Note that Eqs. [4.20] and [4.21] contain the integral over V_m with opposite signs. Therefore, this integral will not appear in the sum $\Delta W_m + \Delta W_g$. Hence, in keeping with Eqs. [4.1] and [4.2] one can represent the total energy of capillary interaction in the form

$$\Delta W = \Delta W_w + \Delta\tilde{W}_m + \Delta\tilde{W}_g, \quad [4.23]$$

where $\Delta\tilde{W}_m$ is given by Eq. [4.20] without the integral over V_m:

$$\Delta\tilde{W}_m = \tfrac{1}{2}\gamma J - \gamma\pi r_2^2 - \tfrac{1}{2}\pi\gamma(qr_2)^2\zeta_1^2(s) - \tilde{W}_{m\infty}. \quad [4.24]$$

In Eqs. [4.20] and [4.24] the expressions for J and $\zeta_1(s)$ are given by Eqs. [4.16] and [3.6] for fixed contact angle and Eqs. [4.17] and [3.8] for fixed contact line at the wall. Equation [4.23] along with Eqs. [4.7], [4.22], and [4.24] will be used below to calculate ΔW.

5. FORCE APPROACH

(a) Basic Equations

The force approach to the capillary interactions includes a direct calculation of the forces exerted on the particle, e.g., pressure integrated throughout the particle surface or surface tension integrated along the three-phase contact line (13, 16). In this aspect the force approach is an alternative to the energetic one. On the other hand, these two approaches are equivalent and must give the same numerical results for the capillary force as proven by means of a variational method in Ref. (15). The equivalence of these approaches provides a good numerical test for the correctness of the approximated expressions for the capillary interaction energy and force derived in this paper.

The net force exerted on the particle is

$$\mathbf{F} = \mathbf{F}^{(\gamma)} + \mathbf{F}^{(w)} + \mathbf{F}^{(p)}, \quad [5.1]$$

where the quantities on the right-hand side are defined after Eq. [3.43]. In fact, the buoyancy (Archimedes) force, $\mathbf{F}^{(p)}$, is a net force due to the hydrostatic pressure, p:

$$\mathbf{F}^{(p)} = -\oint_{S_2} ds\mathbf{n}p \quad [5.2]$$

Here S_2 denotes the particle surface with running outer unit normal $\mathbf{n}$. Similarly, the net force due to the surface tension, $\mathbf{F}^{(\gamma)}$, can be represented in the form

$$\mathbf{F}^{(\gamma)} = \oint_{L_2} dl\boldsymbol{\gamma}, \quad [5.3]$$

where $\boldsymbol{\gamma}$ is the meniscus interfacial tension vector, acting on the contact line L_2 at the particle surface.

The tangentially resolved net force acting on the particle must be equal to the negative derivative of the capillary interaction energy,

$$F_t = \mathbf{t}\cdot\mathbf{F} = -\frac{d\Delta W}{dl} \approx -\frac{d\Delta W}{ds}, \quad [5.4]$$

where $\mathbf{t}$ is the running unit tangent to the generatrix, $\zeta_1(x)$, of the nonperturbed meniscus at the wall, dl is an elementary arc in the interface, and ds is its horizontal projection. Equation [5.4] is the basis for a comparison of the energetic and force approaches. (Note that everywhere in this paper we assume that F_t is exactly balanced by some applied external force; this enables us to work with equilibrium meniscus shape and hydrostatic pressure—otherwise the viscous friction effects should also be taken into account.)

As far as we work with small meniscus slope, we can write

$$\sin\psi \approx \tan\psi = -\left.\frac{d\zeta_1}{dx}\right|_{x=s}, \quad \mathbf{t}\cdot\mathbf{e}_x = \cos\psi \approx 1, \quad [5.5]$$

where angle ψ characterizes the meniscus slope. From Eqs. [3.43], [5.1], [5.4], and [5.5] it follows that the x component of the net force, F_x, is

$$F_x = \mathbf{e}_x\cdot[\mathbf{F}^{(\gamma)} + \mathbf{F}^{(w)} + \mathbf{F}^{(p)}] = F_t\cos\psi \approx F_t. \quad [5.6]$$

This allows us to calculate F_x (instead of F_t) by using a method similar to the one developed in our previous study, Ref. (13). As the weight is directed along the vertical, $F_x^{(w)} = 0$ and

$$F_x = F_x^{(\gamma)} + F_x^{(p)}. \quad [5.7]$$

For calculation of $F_x^{(p)}$ one can directly use Eq. [6.18] in Ref. (13),

$$F_x^{(p)} = \Delta\rho g r_2 \int_0^\pi d\varphi\cos\varphi\zeta^2(\varphi), \quad [5.8]$$

where φ is the azimuthal angle, which provides a parametrization of the circumference C_2 in the plane xy. Note that ζ includes contributions from both ζ_0 and ζ_1—cf. Eq. [3.2]. Sometimes it is more convenient to use parametrization of C_2 by σ—see Eq. [3.10]. The connection between φ and σ reads (Ref. (16))

$$\cos\sigma = \frac{s\cos\varphi + r_2}{s + r_2\cos\varphi}, \quad \frac{d\sigma}{d\varphi} = \frac{a}{s + r_2\cos\varphi} \qquad [5.9]$$

$$0 \leqslant \sigma \leqslant \pi, \qquad 0 \leqslant \varphi \leqslant \pi.$$

Let us proceed now with calculation of the force due to the interfacial tension. To take into account the presence of an inclined meniscus at the wall we should modify the method developed in Ref. (13). For the sake of clarity we consider the force acting on a cylinder of radius r_2, whose axis is directed along the normal to the surface $\zeta_1(x)$ and passes through the particle center—see Fig. 6. The angle between the running unit normal to the cylinder surface, η, and the surface tension vector, γ, is equal to ψ_2 in each point of the three-phase contact line. Since the boundary condition (Eq. [3.46]) for the spherical particle and this (fictitious) cylinder are the same, the shape of the three-phase contact line and the force, $\mathbf{F}^{(\gamma)}$, will also be the same in both cases.

Let us introduce a new coordinate system (x', y', z') whose z' axis coincides with the cylinder axis—see Fig. 6. The unit basis vectors of the new coordinate system read

$$\mathbf{e}'_x = \mathbf{e}_x\cos\psi - \mathbf{e}_z\sin\psi$$
$$\mathbf{e}'_y = \mathbf{e}_y$$
$$\mathbf{e}'_z = \mathbf{e}_z\cos\psi + \mathbf{e}_x\sin\psi. \qquad [5.10]$$

In this coordinate system the linear element, dl, along the contact line and its running unit tangent, ξ, can be expressed (see Eq. [5.5] and Fig. 6)

$$dl = r_2\chi d\varphi, \quad \chi = \left[1 + \left(\frac{1}{r_2}\frac{d\zeta_0}{d\varphi}\right)^2\right]^{1/2} \qquad [5.11]$$

$$\xi = \frac{1}{\chi}\left[-\sin\varphi\mathbf{e}'_x + \cos\varphi\mathbf{e}'_y + \frac{1}{r_2}\frac{d\zeta_0}{d\varphi}\mathbf{e}'_z\right]. \qquad [5.12]$$

The vector of the running unit normal to the cylinder surface is

$$\eta = \cos\varphi\mathbf{e}'_x + \sin\varphi\mathbf{e}'_y. \qquad [5.13]$$

At a given point M of the contact line one can define the vector of the running unit binormal:

$$\mathbf{b} = \xi \times \eta \qquad [5.14]$$

The vector γ belongs to the plane, formed by the vectors η and $\mathbf{b}$

$$\gamma = \gamma(\sin\psi_2\mathbf{b} + \cos\psi_2\eta) \qquad [5.15]$$

By using Eqs. [5.10]–[5.15] we obtain the following expression for the x component of the interfacial tension vector acting on the contact line:

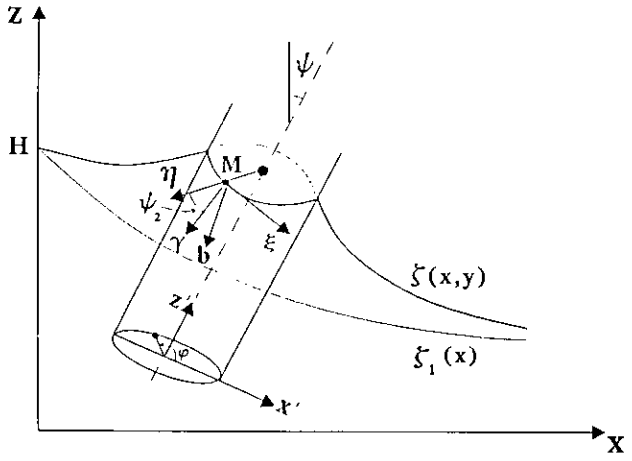

FIG. 6. Sketch of the system used for derivation of the expression for $F_x^{(\gamma)}$: fictitious cylinder of radius r_2 whose axis (perpendicular to $\zeta_1(x)$) passes through the particle center.

$$\gamma_x = \mathbf{e}_x\cdot\gamma = \gamma\left[\cos\psi\left(-\frac{1}{\chi r_2}\frac{d\zeta_0}{d\varphi}\sin\varphi\sin\psi_2 + \cos\psi_2\cos\varphi\right) - \frac{1}{\chi}\sin\psi\sin\psi_2\right].$$

Finally, we obtain (see Eqs. [5.3] and [5.6])

$$F_x^{(\gamma)} = \int_{L_2}\gamma_x dl = -2\pi\gamma r_2\sin\psi_2\sin\psi - 2\gamma\sin\psi_2\int_0^\pi\frac{d\zeta_0}{d\varphi}\sin\varphi d\varphi + \Delta F_x^{(\gamma)}, \qquad [5.16]$$

where

$$\Delta F_x^{(\gamma)} = 2\gamma r_2\cos\psi_2\cos\psi\int_0^\pi\chi\cos\varphi d\varphi \approx \frac{\gamma}{r_2}\int_0^\pi\left(\frac{d\zeta_0}{d\varphi}\right)^2\cos\varphi d\varphi \qquad [5.17]$$

ζ_0 is given by Eq. [3.22] in the case of fixed contact angle and by Eq. [3.29] in the case of fixed contact line at the wall surface. For $\sin\psi$ one should use Eq. [5.5] along with Eq. [3.6] (fixed contact angle) or Eq. [3.8] (fixed contact line).

(b) Asymptotic Expression for F_t

To specify the system, let us consider the case of fixed contact angle at the wall. Then from Eq. [3.6] one obtains

$$\sin\psi \approx \tan\psi = -\left.\frac{d\zeta_1}{\partial x}\right|_{x=s} = \tan\psi_1 e^{-qs}. \qquad [5.18]$$

As shown in Refs. (11, 16) the asymptotic form at large separations of the second term in Eq. [5.16] is given by Eq. [2.15]. The last term in Eq. [5.16] is negligible at large distances.

To estimate $F_x^{(p)}$ one can use the approximation in Eq. [5.8],

$$\zeta(\varphi) \approx h_2 + \frac{dh_2}{ds} r_2 \cos\varphi, \qquad [5.20]$$

to obtain

$$F_x^{(p)} \approx \pi\gamma(qr_2)^2 h_2 \frac{dh_2}{ds}, \; r_2 \ll s, \qquad [5.21]$$

where

$$h_2 \approx q^{-1}\tan\psi_1 e^{-qs} + h_{2\infty} + Q_2 K_0(2qs), \; r_2 \ll s \qquad [5.22]$$

$$\frac{dh_2}{ds} \approx -\tan\psi_1 e^{-qs} - 2qQ_2K_1(2qs), \; r_2 \ll s. \qquad [5.23]$$

For not extremely small ψ_1 and not-too-large capillary charges, Q_2, Eq. [5.21] reduces to

$$F_x^{(p)} \approx -\pi\gamma q(r_2\tan\psi_1 e^{-qs})^2, \quad r_2 \ll s. \qquad [5.24]$$

In fact, for comparatively heavy particles, Eq. [5.24] does not describe well $F_x^{(p)}$ but in this case $F_x^{(p)}$ is negligible in comparison with $F_x^{(\gamma)}$ in Eq. [5.7]. However, if the capillary charge, Q_2, is small ($D_2 \sim 1$), $F_x^{(p)}$ has significant contribution to the total capillary force. In this case we recommend the use of the more rigorous Eq. [5.21] instead of Eq. [5.24]. The combination of Eqs. [2.15], [5.16], [5.18], and [5.24] leads to

$$F_t \approx F_x = -\pi\gamma[2qQ_2^2K_1(2qs) + 2Q_2\tan\psi_1 e^{-qs} + q(r_2\tan\psi_1 e^{-qs})^2] \times [1 + O(q^2R_2^2)], \; r_2 \ll s. \qquad [5.25]$$

In the limit $\psi_1 \to 0$, Eq. [5.25] reduces to the pure capillary image force, given by Eq. [2.15]. The image force (the first term in the brackets in Eq. [5.25]) is proportional to $Q_2^2 \propto R_2^6$—see Eq. [2.12]. This strong dependence of the lateral capillary force on the particle radius is typical for floating particles—cf. Ref. (11).

The second term in the brackets in Eq. [5.25] is proportional to $Q_2 \propto R_2^3$, i.e., to the particle volume. This term originates from the superposition of the particle weight and the upthrust (Archimedes force). This term corresponds to an effective particle–wall *repulsion* or *attraction* depending on the sign of the product $Q_2\tan\psi_1$.

The third term in the brackets in Eq. [5.25] is proportional to πr_2^2, i.e., to the area encircled by the contact line. This term takes into account the pressure jump across the interface. The respective force can be estimated by multiplying the area πr_2^2 by the hydrostatic pressure $\Delta\rho g h_2$ and by $\sin\psi \approx \tan\psi_1 e^{-qs}$ to take projection along the tangent $\mathbf{t}$. Taking into account that $h_2 \approx q^{-1}\tan\psi_1 e^{-qs}$ and $\Delta\rho g = \gamma q^2$, one thus obtains the last term in Eq. [5.25]. Note that this term always corresponds to an effective particle–wall attraction because the product $h_2\tan\psi_1$ is positive for both convex and concave menisci—cf. Figs. 2 and 3.

Similarly, from Eqs. [2.15], [3.8], [3.36], [3.39], and [5.24] one can obtain an asymptotic expression for F_t in the case of fixed contact line at the wall:

$$F_t \approx F_x = -\pi\gamma[-2qQ_2^2K_1(2qs) + 2Q_2qHe^{-qs} + q(r_2qHe^{-qs})^2] \times [1 + O(q^2R_2^2)], \; r_2 \ll s. \qquad [5.26]$$

The physical interpretation of the different terms in Eq. [5.26] is similar to that in Eq. [5.25]. The only difference is that the capillary image force is now repulsive.

In Appendix II we show analytically that the same asymptotic formulas for F_t can be deduced from the general expression for the capillary interaction energy, Eq. [4.23]. In other words, the energetical and force approaches lead to the same asymptotical expression for F_t as it should be expected.

6. NUMERICAL RESULTS AND DISCUSSION

(a) Procedure of Calculations

(i) We suppose that the material parameters ρ_1, ρ_{II}, ρ_2, γ, and α_2, as well as the geometrical parameters R_2 and s, are known. Then from Eqs. [2.1] and [2.13] q and D_2 are calculated. We assume that the parameters ψ_1 or H are known in the cases of fixed contact angle or line, respectively—see Figs. 2 and 3. Note that ψ_1 and H can be both positive and negative; say, in Fig. 2 ψ_1 is positive, whereas in Fig. 3, H is negative.

(ii) Equations [2.6], [3.35], [3.44], [3.45], and [3.50] form a set of five equations for the five unknown variables r_2, Q_2, h_2, ψ_2, and b_2. Equation [3.42] should be used instead of Eq. [3.35] when the contact line (not the contact angle) is fixed at the wall. We use the following iterative procedure in order to solve this set of five equations:

(1) As a first step, an initial guess for r_2 and ψ_2:$Q_2^{(0)}$ is calculated from Eq. [2.12] and

$$r_2^{(0)} = R_2\sin\alpha_2, \quad \psi_2^{(0)} = 0;$$

(2) $Q_2^{(k+1)}$ is calculated from Eq. [2.6];

(3) $h_2^{(k+1)}$ is calculated by means of Eq. [3.35] or Eq. [3.42], depending on the physical situation (fixed contact angle or contact line at the wall);

(4) $b_2^{(k+1)}$ is calculated from Eq. [3.44];

(5) $r_2^{(k+1)}$ is calculated from Eq. [3.45];

(6) $\psi_2^{(k+1)}$ is calculated by using Eqs. [2.6] and [3.50];

(7) If $|1 - Q_2^{(k)}/Q_2^{(k+1)}| < \epsilon$, the iteration process stops,

else the next iteration proceeds from point (2). Here ϵ is the relative error of the calculations, which is fixed in advance. We used $\epsilon = 10^{-8}$.

The current values of $Q_2^{(k)}$, $r_2^{(k)}$, $\psi_2^{(k)}$, $b_2^{(k)}$, and $h_2^{(k)}$ are then used for calculation of the capillary force and interaction energy.

(iii) To determine $W_{w\infty}$, $\tilde{W}_{m\infty}$, and $\tilde{W}_{g\infty}$ one needs the limiting values $r_{2\infty}$, $Q_{2\infty}$, $h_{2\infty}$, $\psi_{2\infty}$, and $b_{2\infty}$ for $s \to \infty$. The latter are determined by the same set of five equations in which Eq. [3.35] (or [3.42]) is exchanged with Eq. [3.23].

(iv) By using Eq. [4.23], along with Eqs. [4.7], [4.22], [4.24], and [4.16] (or [4.17]), one determines the capillary interaction energy, ΔW; then the capillary force, $F_t \approx -d\Delta W/ds$, can be calculated by means of numerical differentiation.

(v) An alternative way to determine F_t is to use Eqs. [5.6]–[5.8], [5.16], and [5.17] in conjunction with Eqs. [3.6] and [3.22] (fixed contact angle at the wall), or [3.8] and [3.29] (fixed contact line at the wall).

(b) Numerical Results

As discussed in the previous section, the energetical and force approaches provide two alternative ways for calculation of the capillary force F_t. They should give the same numerical values of F_t only if the approximations for small meniscus slope (Eq. [2.3]) and small particle ($q^2R_2^2 \ll 1$) are satisfied. In order to check the self-consistency of the theory we compare the complete expression for F_t, Eqs. [5.6]–[5.7], with the derivative of the energy, $d\Delta W/ds$, calculated numerically by using Eqs. [4.23]. The results are presented in Table 1 for a heavy particle of radius $R_2 = 400$ μm for the case of fixed contact line at the wall. One sees that the energetical and the force approaches are in very good quantitative agreement. The numerical values of the capillary force calculated by means of the two alternative approaches coincide within a few percent except at a distance $qs \approx 0.5$ where the force is very close to zero.

In order to check the accuracy of our asymptotic expression for h_2, Eq. [3.42], we have compared it numerically with the rigorous one calculated by substituting the expression for ζ_0, Eq. [3.29], in Eq. [3.36]. One sees in Table 1 that their numerical values are in very good agreement for all values of qs.

We will restrict our numerical study only to the most interesting cases of nonmonotonic capillary interaction between a floating particle and a wall. The behavior of the capillary force in the other situations is trivial and can be easily calculated and interpreted by using the asymptotic expressions, Eqs. [5.25] and [5.26].

Figures 7a and 7b represent the capillary interaction energy, ΔW, vs particle–wall separation, s, for a comparatively large particle of radius $R_2 = 500$ μm and contact angle $\alpha_2 = 70°$. Here and subsequently in the graphics the different couples of curves (solid + dashed) correspond to different mass densities of the floating particle. Mass densities of real substances (mercury, copper, and titanium) are used in the calculations and the particle three-phase contact angle is fixed at $\alpha_2 = 70°$ (different substances can have the same α_2 after an appropriate treatment of their surfaces). The solid curves are calculated by using the more rigorous expression for ΔW, Eq. [4.23], along with Eqs. [4.7], [4.22], and [4.24]. The corresponding dashed curves are calculated by means of the asymptotic expressions derived in Appendix II, Eqs. [B.6] and [B.9]. The case of fixed contact angle at the wall ($\alpha_1 = 89°$) is shown in Fig. 7a, where the capillary interaction energy exhibits a maximum as a function of the separation, s. The value, $s = s^*$, at the energy maximum corresponds to some *nonstable* equilibrium position of the particle. Hence a situation with $s = s^*$ is very difficult to be realized experimentally in this case.

TABLE 1

Comparison of the Lateral Capillary Force, F_t, Eqs. [5.6]–[5.7], with the Derivative $-d\Delta W/ds$ of Eq. [4.23] and of the Expression for h_2, Eq. [3.42], with its Counterpart, Obtained by Means of Numerical Integration of Eq. [3.29] along with Eq. [3.36]

qs	$\Delta W/kT$ ($\times 10^{-10}$)	F_t (N)	$-d\Delta W/ds$ (N)	$h_2/h_{2\infty}$ Eq. [3.42]	$h_2/h_{2\infty}$ Eqs. [3.29] and [3.36]
0.2	−4.699	3.737×10^{-7}	3.613×10^{-7}	0.856	0.849
0.3	−6.441	1.923×10^{-7}	1.815×10^{-7}	0.956	0.952
0.4	−7.261	8.431×10^{-8}	7.633×10^{-8}	1.017	1.014
0.5	−7.544	2.044×10^{-8}	1.485×10^{-8}	1.054	1.052
0.8	−6.961	-5.413×10^{-8}	-5.560×10^{-8}	1.095	1.094
1.0	−6.149	-6.444×10^{-8}	-6.474×10^{-8}	1.095	1.095
2.0	−2.612	-3.772×10^{-8}	-3.716×10^{-8}	1.049	1.049
3.0	−0.994	-1.506×10^{-8}	-1.480×10^{-8}	1.019	1.019
5.0	−0.136	-2.098×10^{-9}	-2.060×10^{-9}	1.003	1.003

Note. The contact line is fixed at the wall. The parameters are $R_2 = 400$ μm, $H = -40$ μm, $\alpha_2 = 70°$, $\rho_2 = 8.9$ g/cm^3, $\rho_1 = 1$ g/cm^3, $\rho_{II} = 0$, $\gamma = 72.4$ mN/m, $h_{2\infty} = -156.5$ μm, $\psi_{2\infty} = -12.1°$.

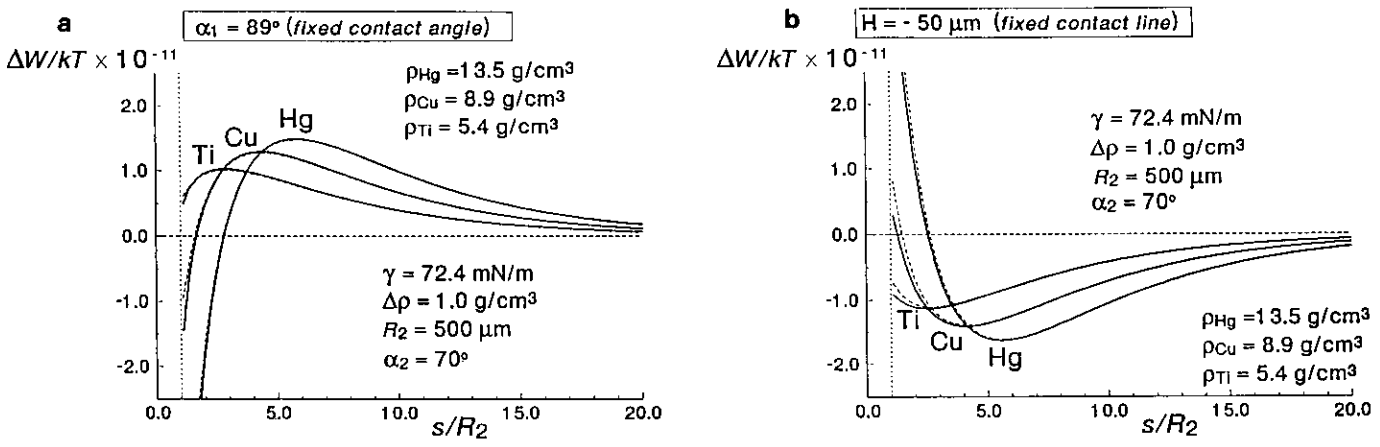

FIG. 7. Plot of the capillary interaction energy, ΔW, vs separation, s, between a particle and a wall: (a) in the case of fixed contact angle at the wall (α_1 = const), and (b) in the case of fixed contact line at the wall (H = const). The three curves correspond to different mass densities of the particle for the same particle contact angle, α_2.

The complementary case of fixed contact line at the wall is illustrated in Fig. 7b where the parameters of the system are the same. Here, the liquid level elevation is $H = -50$ μm. In this case ΔW has a minimum and the particle position $s = s^*$ corresponds to *stable* equilibrium. Note that the equilibrium separation, $s = s^*$, is larger for the heavier particles.

More transparent interpretation of these effects is possible, if we consider the behavior of the lateral capillary force, F_t, acting on the floating particle. In Figs. 8a and 8b, F_t is plotted as a function of the separation, s, for the same configurations and parameters as in the previous plots for ΔW, Figs. 7a and 7b. It is seen in Fig. 8a (for fixed contact angle at the wall) that when approaching the wall, the floating particle meets a force barrier due to its weight (the particle is heavy and the weight force is dominant). However, at $s = s^*$ the particle weight force is exactly counterbalanced by the attractive image force and the particle buoyancy, and F_t is zero—cf. Eq. [5.25]. Below $s = s^*$ the capillary image force dominates and the result is an attraction between the particle and the wall.

The situation, considered in Fig. 8b (fixed contact line at the wall) is just the opposite. Since $H < 0$ and the particle is heavy ($Q_2 < 0$), the particle weight tends to bring the particle closer to the wall. However, the capillary image and the buoyancy force in this case are repulsive and at some separation, $s = s^*$, counterbalance the weight force, giving a stable equilibrium. In this case the magnitude of the equilibrium separation, s^*, is of the order of several millimeters and is a measurable quantity. The value of s^* depends on the particle geometrical and material parameters, R_2, ρ_2, α_2, etc. This fact provides a possibility for experimental verification of the theoretical predictions by measuring of the particle equilibrium position. Besides, the other parameters (H, γ) can be controlled during the experiment. Such experiment

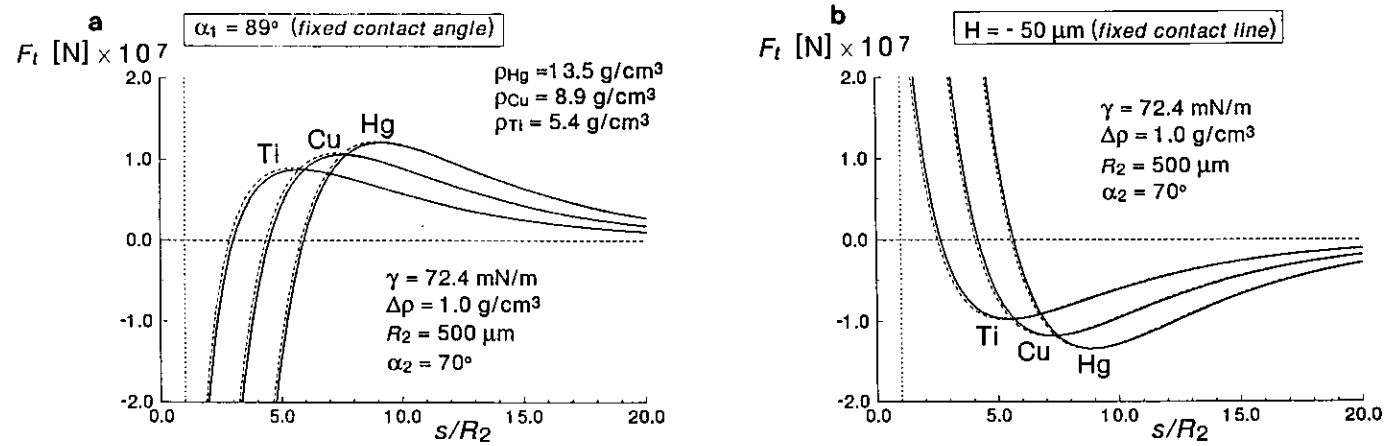

FIG. 8. Plot of the capillary force, F_t, as a function of the particle–wall separation, s, for three different particle mass densities: (a) for fixed contact angle at the wall, and (b) for fixed contact line at the wall.

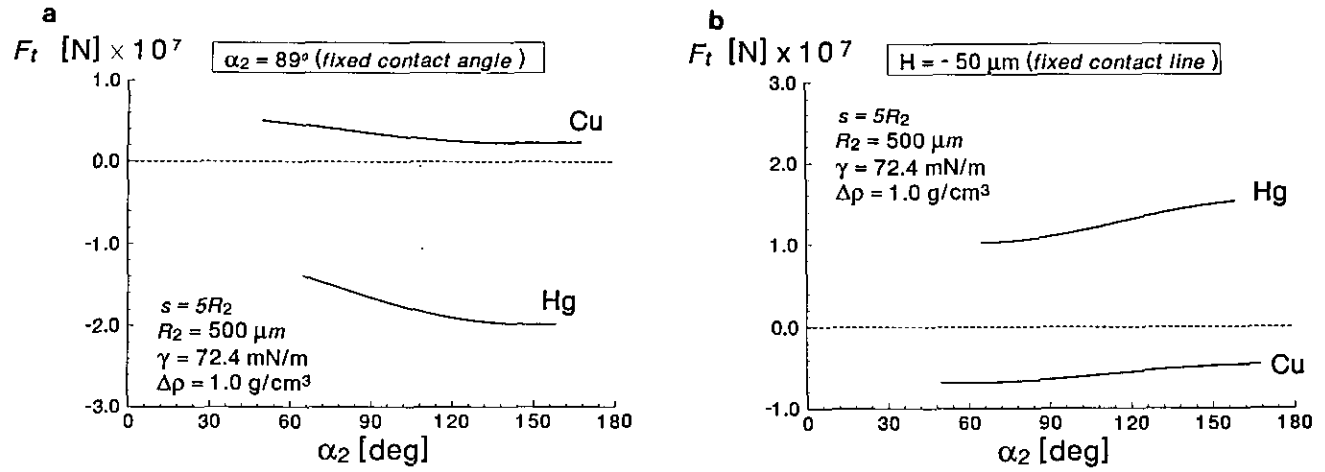

FIG. 9. Lateral capillary force, F_t, as a function of the particle contact angle, α_2 for a fixed particle–wall separation, $s = 2.5R_2$: (a) in the case of fixed contact angle at the wall (α_1 = const), and (b) in the case of fixed contact line at the wall (H = const). The two curves correspond to particle mass density ρ_2 = 8.9 and 13.5 g/cm^3, respectively.

is provided in the second part of this study, where data for submillimeter copper particles and mercury droplets are obtained and interpreted.

The dependence of the lateral capillary force, F_t, on the particle contact angle, α_2, is illustrated in Figs. 9a and 9b for fixed values of the other parameters: particle radius, R_2, and mass density, ρ_2, particle–wall separation, s, etc. The two curves correspond to different particle mass densities. One sees that F_t is weakly dependent on α_2.

Figures 10a and 10b illustrate the dependence of the capillary interaction energy, ΔW, on the particle radius, R_2, for a fixed particle–wall separation, $s = 5R_2$. It is seen that in both cases (α_1 = const, Fig. 10a, and H = const, Fig. 10b) the increase of the particle size leads to a change in the type of interaction: from repulsion to attraction in Fig. 10a and from attraction to repulsion in Fig. 10b. The interpretation is connected with the strong dependence of the image term in Eq. [B.6] and Eq. [B.9] on the particle radius, $Q_2^2 \propto R_2^6$, whereas the other two terms depend more weakly on R_2. The conclusion is that the effect of capillary image force is pronouncedly expressed only for comparatively large particles of high mass density which cause sufficient interfacial deformation.

Note that the energy of particle–wall capillary interaction is of the order of $10^{11}kT$ for the particles considered (kT is the thermal energy). Moreover, the capillary interactions in such system can dominate over the van der Waals, the electrostatic, and other interactions.

7. CONCLUSIONS

In this study we consider theoretically the capillary interaction between a submillimeter particle attached to a fluid

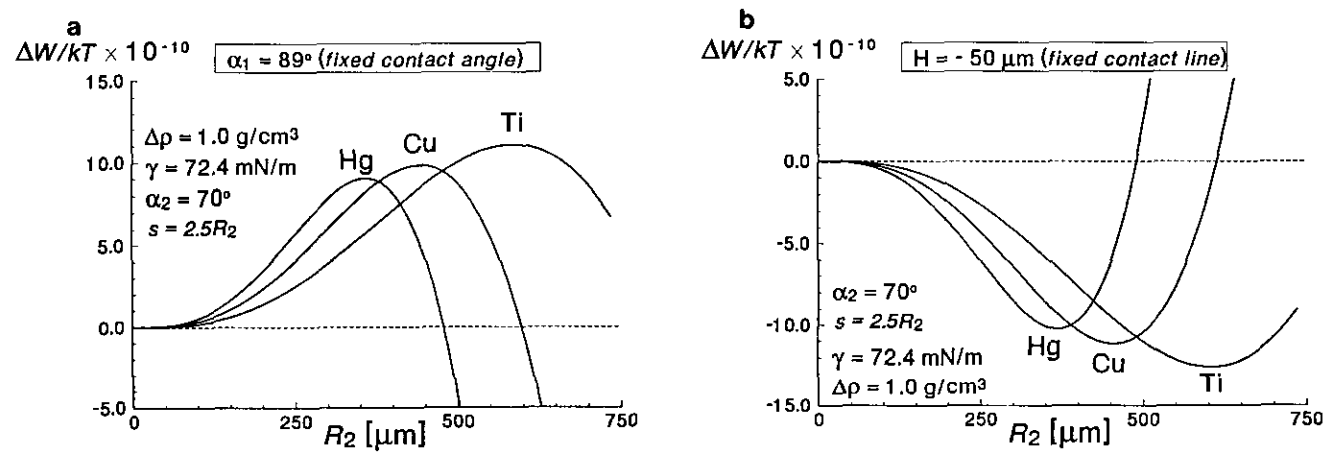

FIG. 10. Capillary interaction energy, ΔW, as a function of the particle radius, R_2, for a given particle–wall separation, $s = 5R_2$: (a) in the case of fixed contact angle at the wall (α_1 = const), and (b) in the case of fixed contact line at the wall (H = const). The three curves correspond to different mass densities of the particle.

interface and a vertical planar wall. Two specific realistic cases are analyzed in detail: (a) constant three-phase contact angle along the wall surface (see Fig. 2) and (b) fixed contact line along the wall (Fig. 3). The main new results can be summarized as follows:

- It is shown that the meniscus deformation, created by a particle floating in a vicinity of a wall, leads to the appearance of a capillary force exerted on the particle. This force is attractive in case (a) and repulsive in case (b)—see Section 2 and Fig. 1. Since this force is similar in several aspects to the image forces in electrostatics, we call it "capillary image force."
- The interplay of the capillary image force, gravity, and buoyancy (Archimedes) force can lead to a nonmonotonic net interaction between the particle and the wall. In particular, in case (a) one can observe a maximum in the curve of the interaction energy, ΔW, vs distance, s, which corresponds to attraction at small distances and repulsion at large separations. More interesting is case (b) where a minimum in the dependence $\Delta W(s)$ can exist. Thus an equilibrium stable position of the particle can be observed.
- The shape of the particle three-phase contact line was determined (Section 3), which is necessary for calculation of the interaction energy and force. The latter were calculated by following two alternative general approaches (the energetical and force approaches, respectively) proposed in Ref. (13). The numerical agreement of the results stemming from these two approaches is very good, which is an additional support of the self-consistency of the used approximations.
- For not-too-small separations simpler and shorter asymptotic expressions for the interaction energy and force are derived—see Eqs. [5.25] and [B.6] for case (a) and Eqs. [5.26] and [B.9] for case (b). The numerical comparison of the exact and the asymptotic expressions performed in Section 6 (see Figs. 7 and 8) shows a very good agreement, except for the region of small particle–wall separation.

Some of the predictions of this study are experimentally observed and quantitatively verified in the second part of this work, Ref. (17).

APPENDIX I. DERIVATION OF EXPRESSIONS FOR ΔA_w AND J

(a) Uniformly Valid Expression for ΔA_w

Eq. [3.4] in Ref. (16) gives an asymptotic expression for ΔA_w, which is valid at small particle–wall separations:

$$\Delta A_w = 2\pi Q_2 q^{-1}(1 - qa), (qa)^2 \ll 1. \qquad [A.1]$$

On the other hand, for large separations, $(qa)^2 \geqslant 1$, by substituting Eq. [3.15] with "+" into Eq. [4.5] one obtains

$$\Delta A_w = 4Q_2 \int_0^\infty K_0(q\sqrt{y^2 + s^2})dy$$

$$= 4Q_2 \int_s^\infty K_0(qt) \frac{tdt}{\sqrt{t^2 - s^2}}. \qquad [A.2]$$

The integral in Eq. [A.2] can be solved analytically (see Ref. (24)); the result reads

$$\Delta A_w = 2\pi Q_2 q^{-1} e^{-qs}, \quad (qa)^2 \geqslant 1. \qquad [A.3]$$

For large separations, $(qa)^2 \geqslant 1$, between small particles, $(qr_2)^2 \ll 1$, one has $s \approx a$—see Eq. [3.11]. Then by comparing Eqs. [A.1] and [A.3] one obtains Eq. [4.6], which can be used for all values of the particle–wall separation. Note that all expressions for ΔA_w discussed above are pertinent to the case of fixed contact angle at the wall, when the boundary condition [2.5] holds. In the alternative case of fixed contact line at the wall (i.e., Eq. [2.8] holds) ΔA_w is identically zero.

Concerning integral J defined by Eq. [4.15], one can write

$$J = J_1 + J_2, \qquad [A.4]$$

where

$$J_k = -\oint_{C_k} dl(\zeta + \zeta_1)\boldsymbol{\mu} \cdot \nabla_{II}\zeta_0, \; k = 1, 2. \qquad [A.5]$$

(b) Uniformly Valid Expression for J_1

Let us first consider the case of fixed contact angle at the wall. In this case from Eq. [3.5] one obtains

$$\boldsymbol{\mu} \cdot \nabla_{II}\zeta_0 = 0, \quad (\text{on contour } C_1). \qquad [A.6]$$

Hence

$$J_1 = 0 \quad (\text{fixed contact angle at the wall}). \qquad [A.7]$$

Let us proceed with the case of fixed contact line at the wall. Equations [3.7] and [A.5] yield

$$J_1 = -2H \oint_{C_1} dl\boldsymbol{\mu} \cdot \nabla_{II}\zeta_0. \qquad [A.8]$$

On the other hand, for $(qs)^2 \geqslant 1$ from Eq. [3.15] (with "−") and Eq. [3.16] one obtains

$$\boldsymbol{\mu} \cdot \nabla_{II}\zeta_0|_{x=0} = \left.\frac{\partial \zeta_0}{\partial x}\right|_{x=0}$$

$$= 2qQ_2 \frac{s}{\sqrt{s^2 + y^2}} K_1(q\sqrt{s^2 + y^2}). \qquad [A.9]$$

From Eqs. [A.8] and [A.9] one obtains

$$-J_1 = 4H\int_0^\infty dy\,\frac{\partial\zeta_0}{\partial x}\bigg|_{x=0} = 8HQ_2qs\int_s^\infty \frac{K_1(qt)dt}{\sqrt{t^2-s^2}}. \qquad [A.10]$$

The last integral in Eq. [A.10] can be solved (see Ref. (24)) to yield

$$J_1 = -2\pi HQ_2e^{-qs}\ \text{(fixed contact line at the wall)}. \qquad [A.11]$$

Formally, we derived Eq. [A.11] for $qs \geqslant 1$. However, for $(qs)^2 \ll 1$, Eq. [A.11] gives the correct limit ($J_1 = -2\pi HQ_2$) obtained by substituting Eq. [2.39] from Ref. (13) with $Q_1 = -Q_2$ into Eq. [A.8]. Hence one can use Eq. [A.11] for the whole range of particle–wall separations.

(c) Uniformly Valid Expression for J_2

In keeping with Eqs. [3.2] and [A.5] one can write

$$J_2 = -\oint_{C_2} dl(\zeta+\zeta_1)\boldsymbol{\mu}\cdot\nabla_{\mathrm{II}}\zeta_0. \qquad [A.12]$$

Since $\boldsymbol{\mu} = \mathbf{e}_r$, having in mind Eqs. [2.6], [2.11], and [3.46], one can transform Eq. [A.12] to read

$$J_2 = 2\pi Q_2h_2 - \oint_{C_2} dl\zeta_1\boldsymbol{\mu}\cdot\nabla_{\mathrm{II}}\zeta_0 = 2\pi Q_2h_2 + \frac{Q_2}{r_2}\oint_{C_2} dl\zeta_1. \qquad [A.13]$$

By using polar coordinates

$$x = s + r\cos\varphi, \quad 0 \leqslant \varphi \leqslant 2\pi, \qquad [A.14]$$

and accounting for Eqs. [3.6] and [3.8], one can represent the integral in Eq. [A.13],

$$\oint_{C_2} dl\zeta_1 = 2r_2Ae^{-qs}\int_0^\pi e^{-qr_2\cos\varphi}d\varphi = 2\pi r_2Ae^{-qs}[1+O(q^2r_2^2)], \qquad [A.15]$$

where φ is the azimuthal angle which provides a parametrization of the circumference C_2 and

$$A \equiv \begin{cases} q^{-1}\tan\psi_1 & \text{for fixed contact angle} \\ H & \text{for fixed contact line.} \end{cases} \qquad [A.16]$$

The combination of Eqs. [A.4], [A.7] (or [A.11]), [A.13], [A.15], and [A.16] gives the uniform expressions for J, Eqs. [4.16]–[4.17].

APPENDIX II. ASYMPTOTIC EXPRESSION FOR ΔW

The tangential component of the capillary force exerted on the particle is

$$F_t = \mathbf{t}\cdot\mathbf{F} = -\frac{d\Delta W}{dl} \approx -\frac{d\Delta W}{ds}, \qquad [B.1]$$

where $\mathbf{t}$ is the running unit tangent to the generatrix, $\zeta_1(x)$, of the nondisturbed meniscus at the wall; dl is elementary length along the generatrix, because of the small meniscus slope $dl = ds/\cos\psi \approx ds$, where ds is element along the x axis.

According to Eq. [6.3] in Ref. (11), for a floating particle one can write

$$\frac{db_2}{ds} = -r_2\frac{d\psi_2}{ds} = \frac{1}{2}\frac{r_2}{R_2-b_2}\frac{dr_2}{ds} = -\frac{dQ_2}{ds} \times [1+O(q^2R_2^2)] = \frac{1}{2}(qr_2)^2\frac{dh_2}{ds}[1+O(q^2R_2^2)]. \qquad [B.2]$$

Equation [B.2] will help us to carry out the differentiation in Eq. [B.1].

Let us first consider the case of fixed contact angle at the wall. In this case from Eqs. [4.7], [4.16], [4.22]–[4.24], and [B.2], one derives

$$\frac{d\Delta W_{\mathrm{w}}}{ds} = \pi\gamma\left[-(qr_2)^2R_2\cos\alpha_2\frac{dh_2}{ds} + \tan\psi_1\times\left(2Q_2 + qr_2^2\frac{dh_2}{ds}\right)e^{-qs}\right][1+O(q^2R_2^2)] \qquad [B.3]$$

$$\frac{d\Delta\tilde{W}_{\mathrm{m}}}{ds} = \pi\gamma\left\{\left[Q_2 - \frac{1}{2}(qr_2)^2h_2 + (qr_2)^2R_2\cos\alpha_2\right]\times\frac{dh_2}{ds} - \tan\psi_1\left(Q_2+\frac{1}{2}qr_2^2\frac{dh_2}{ds}\right)e^{-qs} + q(r_2\tan\psi_1e^{-qs})^2\right\}[1+O(q^2R_2^2)] \qquad [B.4]$$

$$\frac{d\Delta\tilde{W}_{\mathrm{g}}}{ds} = -2\pi\gamma Q_2\frac{dh_2}{ds}[1+O(q^2R_2^2)]. \qquad [B.5]$$

Finally, a substitution of Eqs. [4.23] and [B.3]–[B.5] along with Eq. [5.23] into Eq. [B.1] leads to Eq. [5.25], i.e., the energetical and force approaches give identical asymptotic expressions.

To find an approximate expression for ΔW one can integrate Eq. [5.25] with constant Q_2 (which is reasonable when $|\zeta_1| \leqslant |\zeta_0|$—see Eq. [3.50] and the comment after it):

$$\Delta W = -\pi\gamma\Big[Q_2^2 K_0(2qs) + 2Q_2 q^{-1}\tan\psi_1 e^{-qs} + \frac{1}{2}(r_2\tan\psi_1 e^{-qs})^2\Big] \times [1 + O(q^2R_2^2)],\ r_2 \ll s \quad [B.6]$$

Note that for small particle–wall separations or very small particles, Eq. [B.6] is not accurate and one should use for calculations the more general expressions Eqs. [4.7] and [4.22]–[4.24].

Let us proceed with the case of fixed contact line at the wall. The analogues of Eqs. [B.3] and [B.4] now read

$$\frac{d\Delta W_w}{ds} = -\pi\gamma(qr_2)^2 R_2\cos\alpha_2 \frac{dh_2}{ds}[1 + O(q^2R_2^2)] \quad [B.7]$$

$$\frac{d\Delta \tilde{W}_m}{ds} = \pi\gamma\Big\{\Big[Q_2 - \frac{1}{2}(qr_2)^2 h_2 + (qr_2)^2 R_2\cos\alpha_2\Big] \times \frac{dh_2}{ds} + qH\Big(Q_2 + \frac{1}{2}qr_2^2\frac{dh_2}{ds}\Big)e^{-qs} + q(qr_2He^{-qs})^2\Big\}[1 + O(q^2R_2^2)]. \quad [B.8]$$

Equation [B.5] is valid also in the present case of fixed contact line at the wall. Finally, a substitution of Eqs. [4.23], [B.5], [B.7], and [B.8] along with Eqs. [3.36] and [3.39] into Eq. [B.1] leads to Eq. [5.26]—again the energetical and force approaches give the same result. Hence, we have agreement between the energetical and force approaches with respect to the asymptotic expressions for F_t.

By integrating Eq. [5.26] at fixed Q_2 one obtains an approximated expression for ΔW:

$$\Delta W = -\pi\gamma[-Q_2^2 K_0(2qs) + 2Q_2 He^{-qs} + \tfrac{1}{2}(r_2 qHe^{-qs})^2] \times [1 + O(q^2R_2^2)],\ r_2 \ll s. \quad [B.9]$$

ACKNOWLEDGMENT

This work was supported by Nagayama Protein Array Project under the Program "Exploratory Research for Advanced Technology" (ERATO) of the Research and Development Corporation of Japan (JRDC).

REFERENCES

1. Hinsch, K., *J. Colloid Interface Sci.* **92,** 243 (1983).
2. Camoin, C., Roussel, J. F., Faure, R., and Blanc, R., *Europhys. Lett.* **3,** 449 (1987).
3. Gerson, D. F., Zaijc, J. E., and Ouchi, M. D., *in* "Chemistry for Energy" (M. Tomlinson, Ed.), ACS Symp. Series, Vol. 90, p. 77. Am. Chem. Soc., Washington DC, 1979.
4. Henry, J. D., Prudich, M. E., and Vaidyanathan, K. P., *Sep. Purif. Methods* **8,** 81 (1979).
5. Denkov, N. D., Velev, O. D., Kralchevsky, P. A., Ivanov, I. B., Yoshimura, H., and Nagayama, K., *Langmuir* **8,** 3183 (1992).
6. Denkov, N. D., Velev, O. D., Kralchevsky, P. A., Ivanov, I. B., Yoshimura, H., and Nagayama, K., *Nature (London)* **361,** 26 (1993).
7. Nagayama, K., *Nanobiology* **1,** 25 (1992).
8. Gifford, W. A., and Scriven, L. E., *Chem. Eng. Sci.* **26,** 287 (1971).
9. Nicolson, M. M., *Proc. Cambridge Philos. Soc.* **45,** 288 (1949).
10. Chan, D. Y. C., Henry, J. D., and White, L. R., *J. Colloid Interface Sci.* **79,** 410 (1981).
11. Paunov, V. N., Kralchevsky, P. A., Denkov, N. D., and Nagayama, K., *J. Colloid Interface Sci.* **157,** 100 (1993).
12. Kralchevsky, P. A., Paunov, V. N., Ivanov, I. B., and Nagayama, K., *J. Colloid Interface Sci.* **151,** 79 (1992).
13. Kralchevsky, P. A., Paunov, V. N., Denkov, N. D., Ivanov, I. B., and Nagayama, K., *J. Colloid Interface Sci.* **155,** 420 (1993).
14. Velev, O. D., Denkov, N. D., Kralchevsky, P. A., Paunov, V. N., and Nagayama, K., *Langmuir* **9,** 3702 (1993).
15. Kralchevsky, P. A., and Nagayama, K., *Langmuir* **10,** 23 (1994).
16. Paunov, V. N., Kralchevsky, P. A., Denkov, N. D., Ivanov, I. B., and Nagayama, K., *Colloids Surf.* **67,** 119 (1992).
17. Velev, O. D., Denkov, N. D., Paunov, V. N., Kralchevsky, P. A., and Nagayama, K., *J. Colloid Interface Sci.* **166,** 66 (1994).
18. Finn, R., "Equilibrium Capillary Surfaces." Springer-Verlag, New York, 1986.
19. Israelachvili, J. N., "Intermolecular and Surface Forces" (second ed.). Academic Press, New York, 1992.
20. Abramovitz, M., and Stegun, I. A., "Handbook of Mathematical Functions." Dover, New York, 1965.
21. Korn, G. A., and Korn, T. M., "Mathematical Handbook." McGraw–Hill, New York, 1968.
22. Derjaguin, B., *Dokl. Akad. Nauk. USSR* **51,** 517 (1946).
23. Ivanov, I. B., Kralchevsky, P. A., and Nikolov, A. D., *J. Colloid Interface Sci.* **112,** 108 (1986).
24. Prudnikov, A. P., Brichkov, Yu. A., and Marichev, O. I., "Integrals and Series: Special Functions," p. 345. Nauka, Moscow, 1983.
25. Nayfeh, A. H., "Perturbation Methods." Wiley, New York, 1973.
26. McConnell, A. J., "Application of Tensor Analysis." Dover, New York, 1957.